UNIVERSITY OF THESSALY
DEPARTMENT OF MECHANICAL ENGINEERING

CYCLIC PHASE TRANSFORMATIONS AND SOLUTE PARTITIONING IN THE INTERCRITICAL RANGE OF A MEDIUM-MN STEEL

By

Tzini Maria-Ioanna

Supervisor Prof. G. N. Haidemenopoulos

Submitted to the Department of Mechanical Engineering on June 2016 in partial fulfillment of the requirements for the degree of Mechanical Engineer.

Thesis Committee

1st member: (supervisor)	Prof. G. N. Haidemenopoulos Department of Mechanical Engineering, University of Thessaly
2nd member:	Prof. N. Aravas Department of Mechanical Engineering, University of Thessaly
3rd member:	Assistant Prof. A. Kermanidis Department of Mechanical Engineering, University of Thessaly

ABSTRACT

The evolution of austenite fraction and the associated solute partitioning during the intercritical annealing of medium-Mn steels is of great importance for austenite stabilization and the mechanical performance of this class of steels. In the present work, a Fe-0.2C-4.5Mn-0.15Si-0.1Cr-0.25Al (mass%) steel is subjected to a cyclic treatment in the intercritical range ($\alpha+\gamma$) and the evolution of the austenite fraction is measured with dilatometry. A partial phase $\alpha\rightarrow\gamma$ transformation during intercritical annealing was performed in Fe-0.2C-4.5Mn steel in order to investigate the effect of Mn. Additional partial phase transformations $\alpha\rightarrow\gamma$ and $\gamma\rightarrow\alpha$ during intercritical annealing, have been simulated in Fe-0.2C-5Mn, Fe-0.2C-0.2Mn and Fe-0.2C (mass%) steels for comparison. For the case of 4.5Mn steel, the evolution of austenite fraction and solute partitioning are simulated when the starting time of the cyclic treatment is well before the equilibrium fractions have been established in the respective isothermal intercritical treatment. The evolution of austenite during thermal cycling in the intercritical range comprises of forward, inverse and stagnant stages. During inverse transformation the α/γ interface proceeds in a direction opposite to the temperature change. During the stagnant stage the transformation is very sluggish, and proceeds at infinitesimal rate. The fraction of austenite formed decreases in each successive cycle while the kinetics of the evolution of austenite is controlled by the Mn diffusion in ferrite.

The cyclic behavior depends on the starting time of the cyclic thermal treatment relative to the isothermal curve. For a starting time after the final phase equilibrium, the cyclic behavior is characterized by hysteresis loop formation. No loop formation was observed for the plain carbon steel. The forward, inverse and stagnant stages were investigated. The duration of the inverse stage is larger at the minimum temperatures of the cycle, while the phase fraction formed during the inverse stage is larger at the maximum temperature of the cycle. For a starting time before the final phase equilibrium the transformation is characterized as inverse during the whole cooling part and as forward during the heating part of the cycle. The partitioning of Mn and C was examined for the 4.5Mn steel for a case before the equilibrium volume fractions have been established in the isothermal curves. Partitioning of Mn and C take place from ferrite to austenite during the cyclic transformation. Due to the low diffusivity in austenite, wells form in the composition profiles in austenite of both Mn and C. These wells are the locus of the interfacial compositions of austenite, corresponding to the variation of the local equilibrium conditions during the thermal cycle.

TABLE OF CONTENTS

LIST OF FIGURES

LIST OF TABLES

LIST OF SYMBOLS

$\mathbf{f_\alpha}$	Volume fraction of ferrite.
$\mathbf{f_\gamma}$	Volume fraction of austenite.
$\boldsymbol{\alpha \rightarrow \gamma}$	Ferrite to austenite transformation.
$\boldsymbol{\gamma \rightarrow \alpha}$	Austenite to ferrite transformation
POI	Position of interface α/γ.
VOI	Velocity of interface α/γ.
$\mathbf{T_{max}, T_{is}, T_{min}}$	Maximum, isothermal and minimum temperatures of the cycle.
$\boldsymbol{\tau}$	Period of the cycle.
$\mathbf{t_S, t_E}$	Starting and ending time of the cyclic thermal treatment.
HR, CR	Heating and cooling rates of the cyclic thermal treatment.

ACKNOWLEDGEMENTS

I am grateful to Prof. G.N. Haidemenopoulos for his consistent guidance and advice during these years. He ignited in me the interest and the enthusiasm for the research. Mostly I would like to thank him for his trust, as well as the way of thinking he infused into me not only in the scientific field but also on how to be a better person.

I would like to express my appreciation to Dr. Panagiota Sarafoglou for her infinite help and precious advice. I hope she will excuse me for the barrage of questions I subjected her, since this emanates from the fact that she is a great teacher and one of the main reasons that this thesis is possible.

I would like to thank John Aristeidakis for the stimulating discussions and his valuable friendship. Many thanks to Dr. Eleni Kamoutsi for her willingness to help me whenever I faced a problem, as well as for the chocolates and the coffee she was supplying me with, in order to survive. Furthermore, I am thankful to Dr. A. Zervaki and the other members of the laboratory of materials for their constant help.

I am grateful to Prof. N. Aravas and Assistant Prof. A Kermanidis for their guidance during the past years and for serving in my thesis committee.

I would like to thank Prof. W. Bleck and Andreas Stieben from the University of RWTH-Aachen for their contribution in this project. The work has been conducted in the framework of the IKYDA 2014-2015 program "Design rules for 3rd generation advanced high strength steels", which is a collaboration between the University of Thessaly and RWTH-Aachen.

Last but not least, I wish to express my gratitude to my family and my friends for making all these years enjoyable and my appreciation to Lenou for her endless patience and encouragement.

This Thesis is dedicated to Fyodor.

1. INTRODUCTION

Medium-Mn steels constitute the core of the 3rd generation advanced high-strength steels. These steels contain 3-12 mass % manganese and the microstructure consists of an ultrafine ferrite-austenite mixture. Transformation-induced plasticity (TRIP) of the retained austenite is responsible for the enhanced formability in these steels and the excellent combination of strength and ductility [1-4]. The role of retained austenite and especially its fraction and stability have long been identified as of paramount importance in exhibiting beneficial TRIP effects [5-6]. Several processing routes have been developed in order to stabilize the austenite such as quench and partitioning (Q&P) [7-8] process and intercritical annealing [9-15]. During intercritical annealing, the partitioning of manganese and carbon to austenite stabilizes the austenitic phase. Thus understanding the kinetics of phase transformations and solute partitioning during intercritical annealing is a prerequisite to the design of medium-Mn steels.

Cyclic partial phase transformation in the intercritical range has been employed recently to study the growth kinetics and phase transformations in low-Mn and low-C Fe-C-Mn alloys [16-17]. In this work the procedure of thermal cycling in the intercritical range was also applied to investigate austenite growth kinetics in medium-Mn steels. The strategy behind the modeling of cyclic intercritical annealing is that it allows to investigate the growth kinetics without the modeling uncertainties of nucleation being part of the transformation [17]. With this type of modeling, it is possible to accurately describe the interfacial conditions and more importantly the solute partitioning during the $\alpha \rightarrow \gamma$ and $\gamma \rightarrow \alpha$ transformations. In addition the fact that the $\alpha \rightarrow \gamma$ and $\gamma \rightarrow \alpha$ transformations proceeds at different rates isothermally, makes the cyclic phase transformations model adequate for the study of growth kinetics. In the above works [16], an "inverse" transformation stage as well as a "stagnant" stage were identified, in addition to the forward transformation of the $\alpha \rightarrow \gamma$ and $\gamma \rightarrow \alpha$ transformations. The inverse transformation, is defined as the transformation where the α/γ interface proceeds in a direction opposite to the temperature change. During the stagnant stage the transformation is very sluggish, and proceeds at infinitesimal rate. The starting time of the cyclic thermal treatment relative to the respective isothermal transformation curve, has an important effect on cyclic behavior. Therefore, in this work the cyclic phase transformation will be simulated for a starting time before and after thermodynamic equilibrium has been established.

The aim of the present study is to describe the growth during the $\alpha \rightarrow \gamma$ and $\gamma \rightarrow \alpha$ transformations and to investigate in more detail the inverse transformation stage and more specifically the solute partitioning which takes place during such cyclic transformations. The study is performed by simulating the cyclic transformations in the intercritical range and by monitoring the position and the velocity of the α/γ interface with temperature and time. An experimental validation of austenite growth kinetics, during the $\alpha \rightarrow \gamma$ transformation and before the final phase equilibrium, was performed with dilatometric techniques.

2. METHODOLOGY

The material investigated was a medium-Mn steel with composition Fe-0.2C-5Mn (mass%). A lean-Mn Fe-0.2C-0.2Mn and a plain carbon Fe-0.2C steel were also considered as reference materials. The experimental validation provided by IKYDA project and performed on LHD-7 steel with chemical composition Fe-0.2C-4.5Mn-0.15Si-0.1Cr-0.028Al (mass%). Due to the necessary comparison of the experimental and computational results, a Fe-0.2C-4.5Mn steel was employed for the simulations. In order to define the maximum and minimum temperatures of the thermal cycle, the respective isopleth sections at constant Mn compositions were constructed with the Thermo-Calc [18] software using the TCFE6 database, shown in Figure 1.

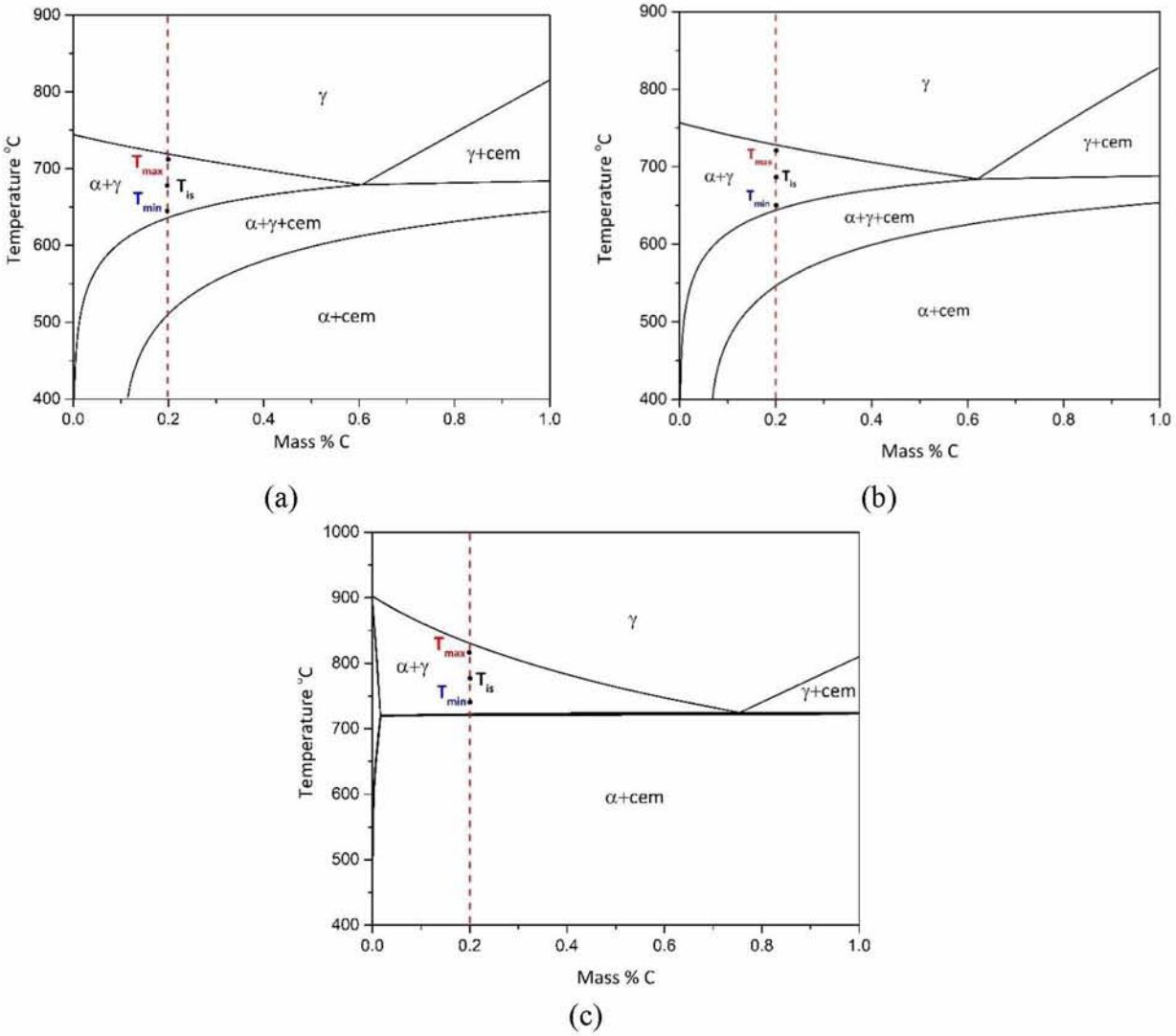

Figure 1: Isopleth sections of (a) Fe-0.2C-5Mn (b) Fe-0.2C-4.5Mn and (c) Fe-0.2C-0.2Mn steels.

The cyclic thermal treatment for the study, is depicted in Figure 2 and the various characteristics of the cycle for each material, are given in Table 1. The cyclic thermal treatment consists of an isothermal holding at T_{is} and three cycles with temperature range between T_{max}

and T_{min}. For the case of 4.5-Mn steel the cycle starts with heating at T_{is}, isothermal holding at this temperature for 2412 sec followed by temperature cycling between T_{max} and T_{min}. The cycling ends with an isothermal holding for 1800 sec and cooling to ambient temperature. The values T_{is}, T_{max} and T_{min} were specifically chosen to span the entire range of the $\alpha+\gamma$ region of the phase diagram. The temperature range $\Delta T = T_{max} - T_{min}$, the heating and cooling rates (HR and CR) were kept constant for the three periods (τ) of the cycle. The equilibrium volume fractions of austenite (f_γ) and ferrite (f_α) at T_{is} are shown in the Table 1, as well.

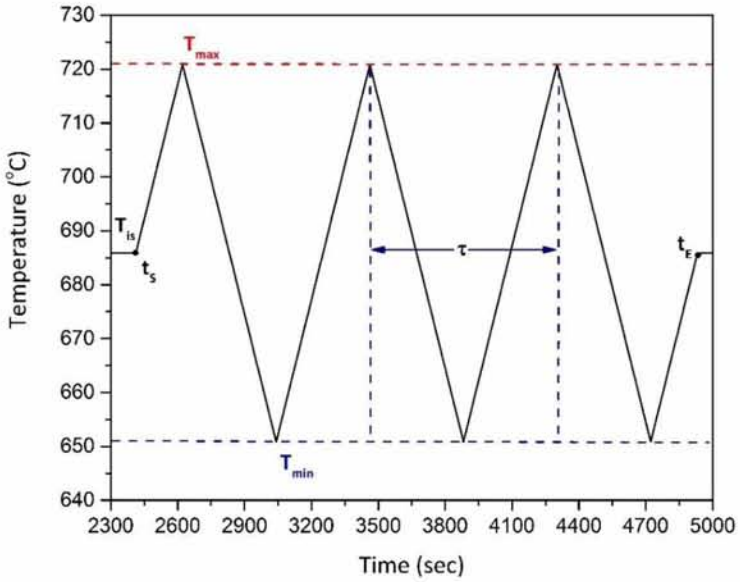

Figures 2: The thermal cycle considered for the simulations and the experiments. T_{is} denotes the isothermal holding temperature, while T_{max} and T_{min} are the maximum and minimum temperatures of the cycle, respectively. The period of the cycle is τ. Time t_S corresponds to the start and time t_E to the end of the cyclic transformation.

Steels	A_1 [°C]	A_3 [°C]	T_{is} [°C]	T_{min} [°C]	T_{max} [°C]	ΔT [°C]	HR, CR [°C min^{-1}]	τ [sec]	f_α	f_γ
Fe-0.2C-5Mn	634	716	675	640	710	70	10	840	0.394	0.605
Fe-0.2C-4.5Mn	644	728	686	651	721	70	10	840	0.394	0.605
Fe-0.2C-0.2Mn	722	828	775	740	810	70	10	840	0.534	0.446
Fe-0.2C	725	835	780	745	815	70	10	840	0.561	0.438

Table 1: The characteristics of the thermal cycle for the steels considered. T_{is} is the isothermal holding temperature, T_{min} and T_{max} are the minimum and maximum temperatures respectively, HR and CR are the heating and cooling rates respectively, τ is the period of the cycle. The volume fractions of ferrite and austenite at T_{is} are f_α and f_γ respectively.

Two cases were considered. The first case is concerned with the $\alpha \rightarrow \gamma$ transformation, corresponding to the intercritical annealing of supersaturated ferrite (martensite) to form austenite. The second case is concerned with the $\gamma \rightarrow \alpha$ transformation, corresponding to ferrite formation from an initially austenitic phase. The 4.5-Mn steel was subjected to cyclic treatment only for the first case, where the evolution of austenite fraction was measured with dilatometry.

The austenite and ferrite growth during the cyclic transformations as well as the associated solute partitioning during intercritical annealing were simulated with the DICTRA software [19] using the MOBFE2 mobility database for ferrous alloys. A single cell planar geometry was employed, shown in Figure 3a and 3b for the $\alpha \rightarrow \gamma$ and $\gamma \rightarrow \alpha$ cases respectively. For the steels investigated a small region size was considered, equal to 1.55 μm corresponding to one-half the measured ferrite to austenite mean distance (center-to-center) [20]. Regarding the 4.5-Mn steel, the total region size depicted in Figure 3c, was taken equal to 1.085 μm, since it was anticipated that the interface movements during the cyclic transformation were going to be small. In addition the solute partitioning is taking place at a small distance from the α/γ interface during the cyclic transformation. A thin austenite slice, 5 nm and 3.5 nm, was attached to the left of the ferrite region in Figure 3a and 3c respectively for the $\alpha \rightarrow \gamma$ case. Correspondingly a thin ferrite slice, 5 nm, was attached to the left of the austenite region in Figure 3b for the $\gamma \rightarrow \alpha$ case. The regions were discretized with a linear grid consisting of 100 grid points and of 150 for the case of 4.5-Mn steel. The initial compositions of austenite slice and ferrite region in Figure 3a and 3c were taken equal to the nominal compositions of the alloy. The same holds for the ferrite slice and austenite region in Figure 3b. Although the compositions in the two phases are identical, the respective activities are not. Diffusional fluxes are generated between the two phases in response to the different activities. Zero flux boundary conditions (closed system) for all elements were imposed at the lower and upper boundaries of the system. Throughout the simulations local equilibrium (LE) conditions were imposed. The parameters monitored were the position of the α/γ interface, which when normalized to the total region size, corresponds to the volume fractions f_α and f_γ of ferrite and austenite for the $\gamma \rightarrow \alpha$ and $\alpha \rightarrow \gamma$ cases respectively, and the velocity of the α/γ interface (VOI). In addition to monitoring the α/γ interface position and velocity, the solute partitioning between the two phases was monitored.

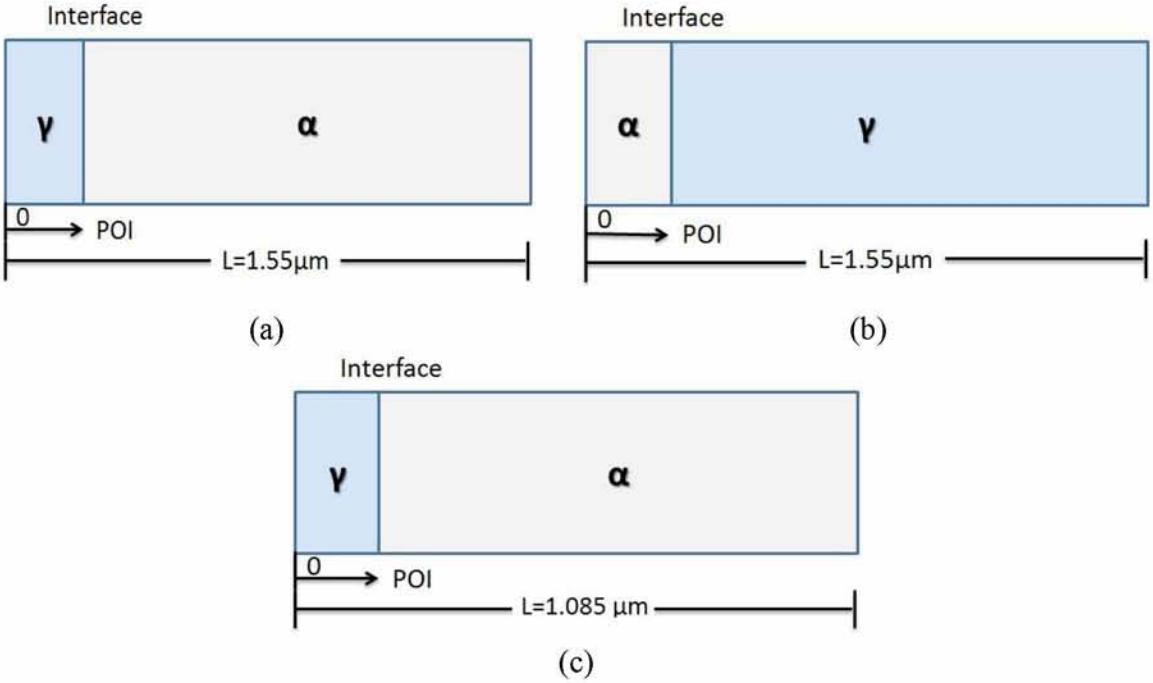

Figure 3: The representative cells employed in the DICTRA simulations of the cyclic transformations (a) for the $\alpha \rightarrow \gamma$, (b) the $\gamma \rightarrow \alpha$ cases accordingly and (c) the $\alpha \rightarrow \gamma$ case for the 4.5-Mn steel. POI denotes the position of the α/γ interface.

For the dilatometric measurements the IKYDA LHD-7 steel was prepared as an 80 kg ingot with a cross-section of 140x140 mm^2 in a vacuum induction melting furnace (2 kHz). The ingots homogenized for 3 hours at 1200 °C and open die forged to a cross-section of 60x60 mm^2. After the forging process, the bars were air cooled to ambient temperature. Before the cyclic thermal treatment, samples with size of 25x40x40 mm^3, were austenitized in a salt bath at 950°C for 1800 sec and quenched in oil. Thermal cycling was performed in the dilatometer according to the schedule of Figure 2. The dilatometer used was a BÄHR DIL805A dilatometer. The specimen used for dilatometry was a solid plate with dimensions 7x4x1.3 mm^3. The volume fraction of austenite was determined by the relative length change by subtracting the linear length change, which is attributed to thermal expansion and contraction.

3. RESULTS

3.1. Cyclic Transformations

3.1.1. Austenite evolution of Fe-0.2C-4.5Mn steel and Experimental Validation.

The isothermal $\alpha \rightarrow \gamma$ and $\gamma \rightarrow \alpha$ transformations in the Fe-0.2C-4.5Mn steel are depicted in Figure 4 for three temperatures 651, 686, 721°C corresponding to the T_{min}, T_{is} and T_{max} of the respective cyclic treatment. The evolution of austenite volume fraction during intercritical annealing takes place in three stages [9, 21, 22]. In stage I, non-partitioning local equilibrium (NPLE) growth of austenite takes place at short times and is controlled by carbon diffusion in ferrite. In stage II, partitioning local equilibrium (PLE) growth of austenite is controlled by manganese diffusion in ferrite, while in stage III, the PLE shrinkage of austenite is controlled by manganese diffusion in austenite. Compared to the $\gamma \rightarrow \alpha$, the $\alpha \rightarrow \gamma$ transformation is considerably faster.

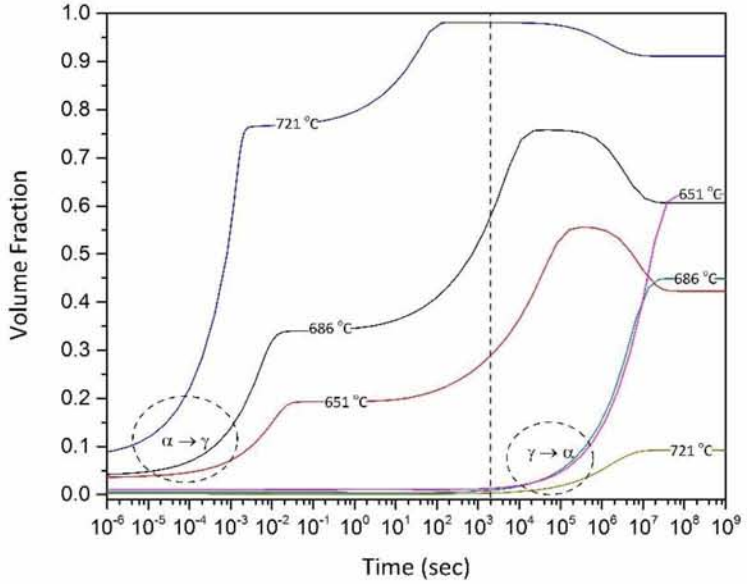

Figure 4: Evolution of the volume fraction of austenite and ferrite for the isothermal $\alpha \rightarrow \gamma$ and $\gamma \rightarrow \alpha$ transformations respectively, in the Fe-0.2C-4.5Mn steel for temperatures 651, 686 and 721°C. The dotted line denotes the starting time t_s =2412 sec of the cyclic transformation.

The dotted line in Figure 4 indicates the starting time (t_s) of the cyclic transformation after the isothermal holding. Following the applied thermal cycle in the dilatometric experiments, a starting time t_s=2412 sec is selected and the $\alpha \rightarrow \gamma$ transformations take place at stage II. It can be deduced from Figure 4 that at this time the $\alpha \rightarrow \gamma$ transformation is still evolving, while the $\gamma \rightarrow \alpha$ transformation is very sluggish.

The evolution of the austenite volume fraction f_γ vs temperature during thermal cycling is depicted in Figure 5. Points S and E on the volume fraction curve, correspond to the start and the end of the cyclic transformation, respectively. Points A, B and C correspond to T_{min} (651°C), whereas points 1, 2 and 3 correspond to T_{max} (721°C). It is observed that the interface does not change direction and the volume fraction is continuously increasing. The parts S-1, A-2, B-3 and C-E on the volume fraction curve, correspond to the "forward" transformation where the f_γ is evolving with the temperature rise. Accordingly, the parts 1-A, 2-B and 3-C′ correspond to the "inverse" transformation, where the interface proceeds in a direction opposite to the temperature change, i.e. austenite is forming during the cooling part of the cycle. Only part C′-C corresponds to a forward transformation, since a small decrease of the f_γ is detected with a decrease in temperature. It is interesting to see that the fraction of austenite formed decreases in each successive cycle. The fractions of austenite formed are 0.07, 0.05 and 0.03 in the 1st, 2nd and 3rd cycles respectively.

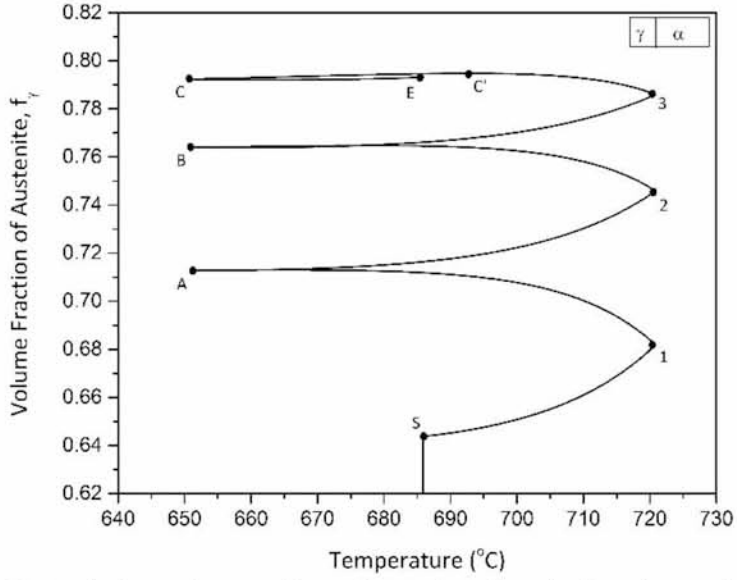

Figure 5: Evolution of austenite volume fraction during thermal cycling in the intercritical range.

In order to explain this behavior, the volume fraction of austenite f_γ, the temperature and the velocity of the interface (VOI) vs. time are depicted in Figure 6. The maxima in the VOI curve correspond to T_{max} while the minima correspond to T_{min}. The VOI decreases in each cycle and this leads to a lower amount of austenite forming in each cycle. The austenite volume fraction curve (f_γ) indicates that each cycle comprises of a forward transformation during heating, an inverse transformation during cooling and a stagnant transformation stage. During the forward transformation, austenite grows as the temperature increases from the minimum to the maximum value of the cycle. At the same time the velocity of the interface increases.

During the inverse transformation, austenite continues to form during the cooling part of the cycle, while at the same time the velocity of the interface decreases. The transition between the forward and inverse transformations takes place at T_{max} where VOI is maximized. At the minimum temperature of the cycle where practically VOI=0, the transformation is sluggish, corresponding to the stagnant transformation stage.

Because at the selected time for the start of the cyclic transformation (t_s=2412 s) the rate of the $\gamma \rightarrow \alpha$ transformation is negligible compared to the rate of the $\alpha \rightarrow \gamma$ transformation, austenite formation during the cooling part of the cycle proceeds entirely by the inverse transformation. However the VOI values in Figure 6 indicate that both transformations, forward and inverse, take place at comparable rates.

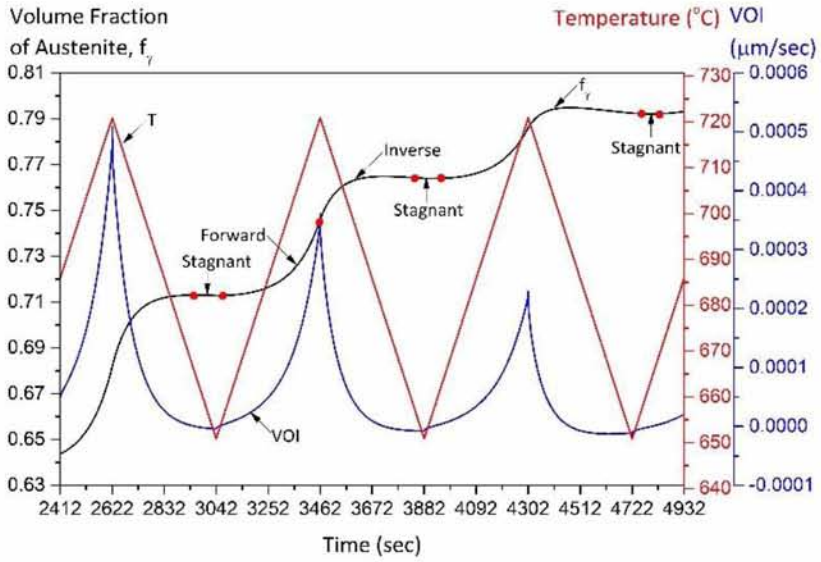

Figure 6: Evolution of austenite volume fraction (f_γ) and velocity of the α/γ interface (VOI) vs. time during thermal cycling in the intercritical range. The forward, inverse and stagnant transformation stages are indicated.

The dilatometric curve obtained from thermal cycling in the dilatometer is shown in Figure 7a. The relative length change is plotted versus temperature. From this curve, the volume fraction austenite is obtained by subtracting the linear thermal expansion and contraction during heating and cooling respectively. This is depicted by the arrows from the dotted lines to the dilatometric curve. The result is shown in Figure 7b, together with the simulation result of Figure 6. The agreement between simulation and experiment is considered good. It appears that the simulation can describe the evolution of the austenite volume fraction during cyclic transformations in the intercritical range.

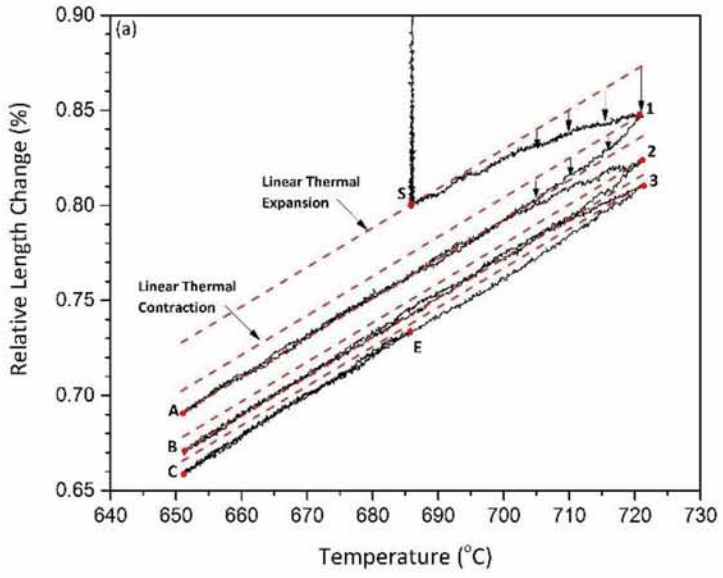

(a)

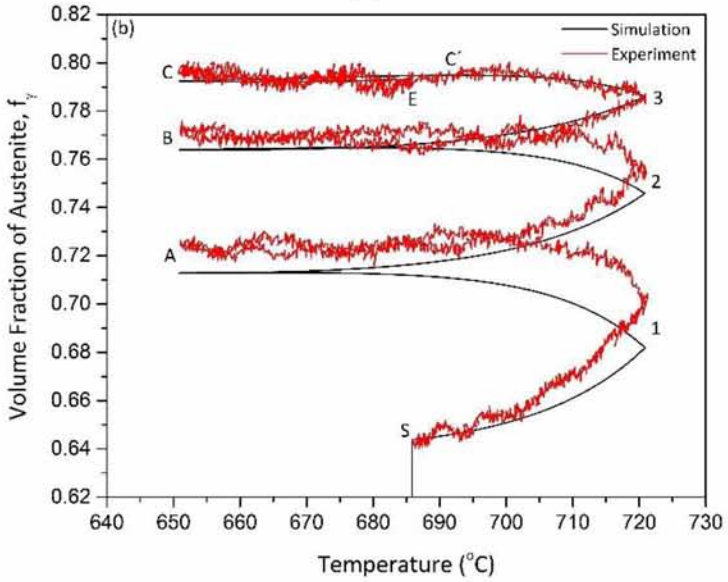

(b)

Figure 7: Dilatometry curves: (a) relative length change vs. T, (b) fraction austenite vs. T (comparison between dilatometry and simulation).

3.1.2. Computational Analysis

3.1.2.1. Fe-0.2C-5Mn steel

The isothermal $\alpha \rightarrow \gamma$ and $\gamma \rightarrow \alpha$ transformations in the Fe-0.2C-5Mn steel are depicted in Figure 8 for three temperatures 640, 675 and 710°C corresponding to the T_{min}, T_{is} and T_{max} of the respective cyclic treatment. Compared to the $\alpha \rightarrow \gamma$, the $\gamma \rightarrow \alpha$ transformation is much slower. Two specific times, t_s, were identified as the start of the cyclic transformations. In the first case $t_s=1x10^8$ sec after equilibrium volume fractions for both austenite and ferrite have been established in the isothermal transformation. At this specific time the PLE shrinkage of austenite is controlled by manganese diffusion in austenite (stage III) [9, 21, 22]. In the second

case, $t_s=2x10^3$ sec, where the $\alpha\rightarrow\gamma$ transformation is evolving while the $\gamma\rightarrow\alpha$ transformation is very sluggish. At this case, the partitioning local equilibrium (PLE) growth is controlled by manganese diffusion in ferrite (stage II). These times are depicted by dotted lines in Figure 8.

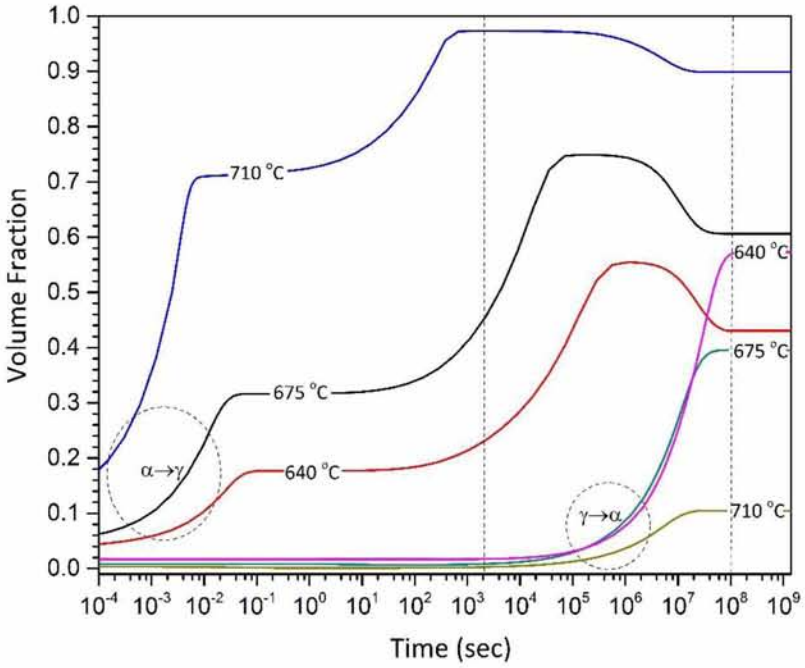

Figure 8: Isothermal $\alpha\rightarrow\gamma$ and $\gamma\rightarrow\alpha$ transformations in the Fe-0.2C-5Mn steel for 640, 675 and 710°C. The dotted lines indicate the starting time of the cyclic transformation.

The cyclic transformations for $t_S=1x10^8$ sec are depicted in Figure 9. The volume fractions f_γ and f_α are plotted as a function of temperature for the $\alpha\rightarrow\gamma$ and $\gamma\rightarrow\alpha$ cases in Figure 9a and 9b respectively. The volume fraction forms hysteresis loops. Point A marks the beginning and point B the end of the cyclic transformation. Regarding Figure 9a, the loops move upwards indicating that more austenite forms at every cycle. In contrast, in Figure 9b the loops move downwards, indicating that more ferrite dissolves, in favor of austenite, at every cycle. An additional feature of the cyclic behavior is the "inverse" transformation, where the transformation proceeds to a direction opposite to the temperature change. This behavior is depicted by CD for T_{max} and EF for T_{min} in Figure 9a and 9b. The temperature range of the inverse transformation $\Delta T_{inv}=T_F-T_E$ at T_{min} is larger than the corresponding $\Delta T_{inv}=T_C-T_D$ at T_{max}. The volume fraction is plotted as a function of time during cycling for the $\alpha\rightarrow\gamma$ and $\gamma\rightarrow\alpha$ cases in Figure 9c and 9d respectively. In the same Figures the variation of temperature (T) and the velocity of the α/γ interface (VOI) are also plotted.

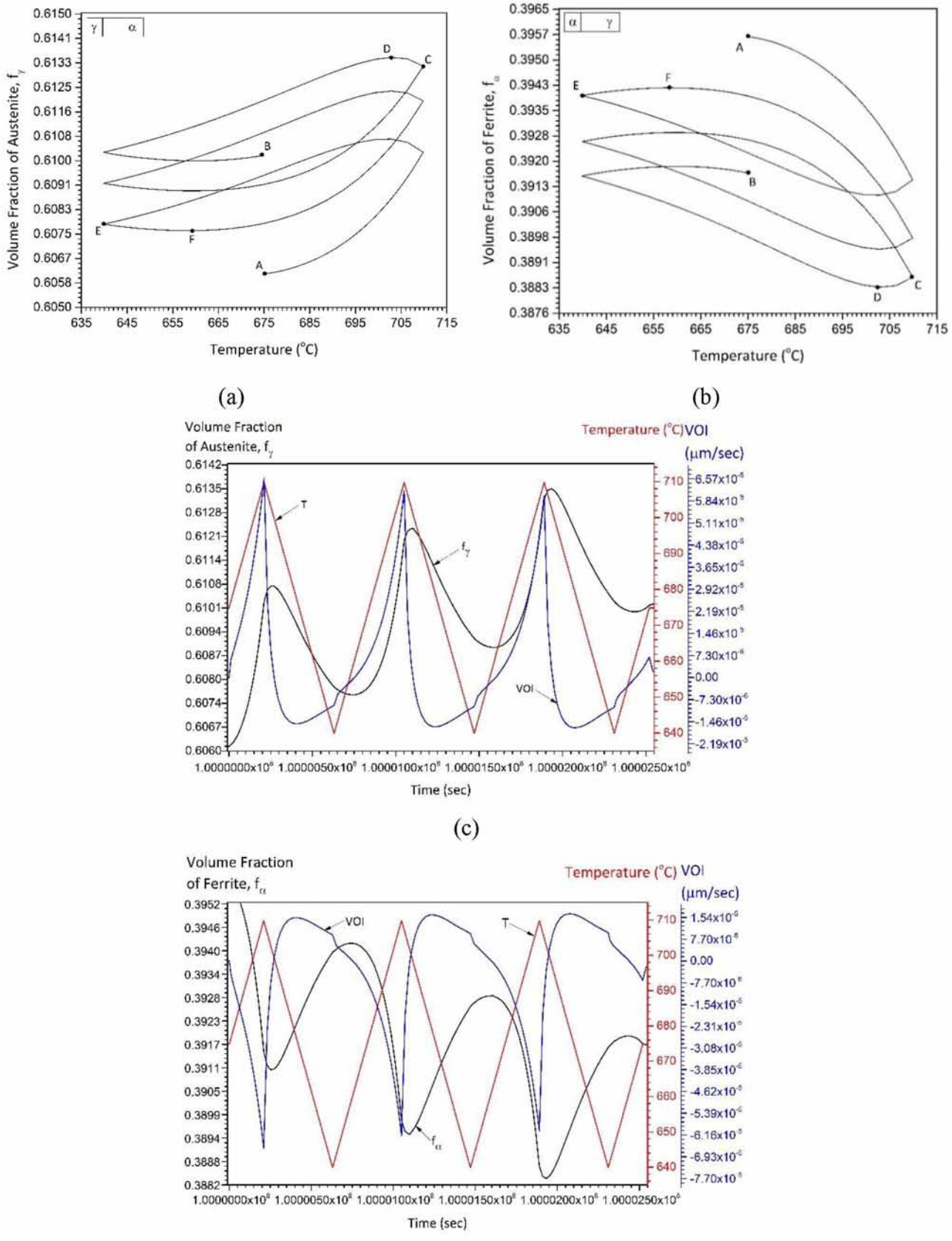

Figure 9: Cyclic transformations in Fe-0.2C-5Mn steel for $t_s=1x10^8$ sec (a) f_γ vs T for the $\alpha\rightarrow\gamma$, (b) f_α vs T for the $\gamma\rightarrow\alpha$, (c) f_γ and VOI vs time for the $\alpha\rightarrow\gamma$ and (d) f_α, VOI vs time for the $\gamma\rightarrow\alpha$ transformations.

The details of the inverse transformation are depicted in a magnified region in the second cycle of Figures 9c and 9d in Figures 10a and 10b respectively for the $\alpha \rightarrow \gamma$ and the $\gamma \rightarrow \alpha$ cases. Point C on the volume fraction curve corresponds to the point of temperature change at T_{max} while point D corresponds to the change of interface direction at VOI=0. Accordingly point E on the volume fraction curve corresponds to the point of temperature change at T_{min} while point F corresponds to the change of interface direction at VOI=0. The duration of the inverse transformation is larger at T_{min}, than the respective duration at T_{max}. The phase fraction formed during the inverse transformation is larger at the maximum temperature of the cycle. A question, which arises, is whether there is a stagnant stage after the inverse transformation stage, where the transformation is sluggish with the temperature change. According to Figure 10 there is no absolute stagnant stage, i.e. a period where VOI=0. The interface is migrating continuously at low velocities even when it changes direction at VOI=0. So a "stagnant stage" characterized by very low interface velocity, is also observed in 5Mn steel.

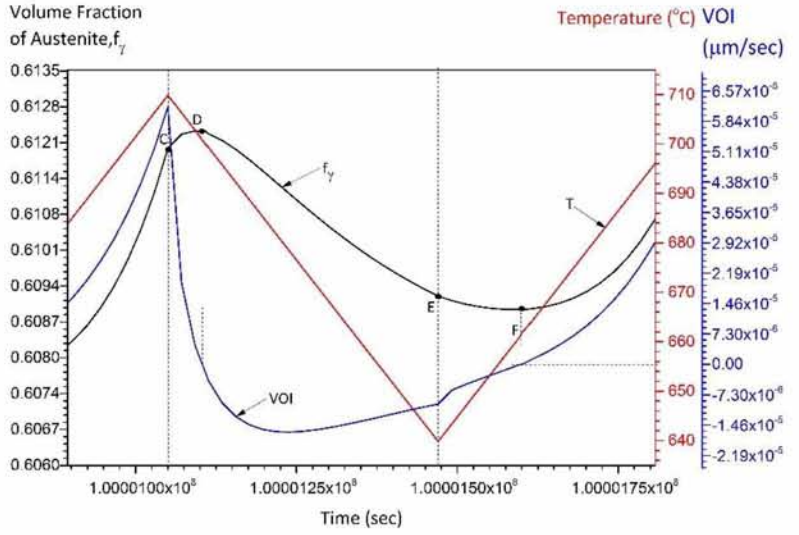

(a)

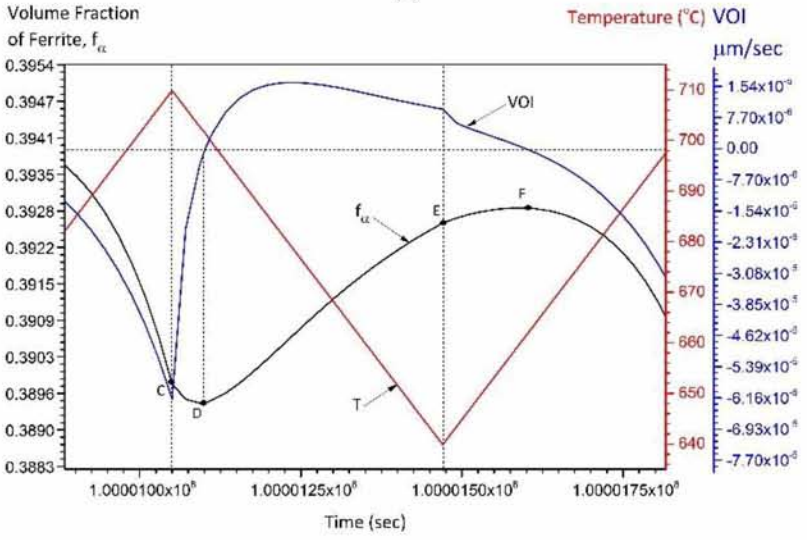

(b)

Figure 10: Magnified regions (second cycle) of Figure 5c and 5d for $\alpha \rightarrow \gamma$ in (a) and $\gamma \rightarrow \alpha$ in (b) respectively, showing the inverse transformation.

The cyclic transformation for $t_s=2x10^3$ sec is depicted for the $\alpha\rightarrow\gamma$ and $\gamma\rightarrow\alpha$ cases in Figure 11. The volume fractions f_γ and f_α are plotted as a function of temperature for the $\alpha\rightarrow\gamma$ and $\gamma\rightarrow\alpha$ transformations in Figure 11a and 11b respectively. In addition, the volume fractions f_γ and f_α, T and VOI vs time for the $\alpha\rightarrow\gamma$ and $\gamma\rightarrow\alpha$ transformations, are shown in Figure 11c and 11d accordingly. Since in this case at $t_s=2x10^3$ sec, the $\gamma\rightarrow\alpha$ transformation during the isothermal treatment (Figure 8) is sluggish, the f_γ during cyclic transformation does not form hysteresis loops. On the contrary the f_γ increases in each cycle, both in the heating and cooling part. In this case austenite forms by inverse transformation during the cooling part of the cycle. On the other hand the f_α during cyclic forms hysteresis loops. The loops move upwards, indicating that more ferrite forms at every cycle. The cyclic behavior resembles of the $\gamma\rightarrow\alpha$ transformation at $t_s=1x10^8$ sec. The duration of the inverse transformation is larger at T_{min}. However, the phase fraction formed during the inverse transformation at T_{max} of the cycle is approximately equal to that formed at T_{min} of the cycle.

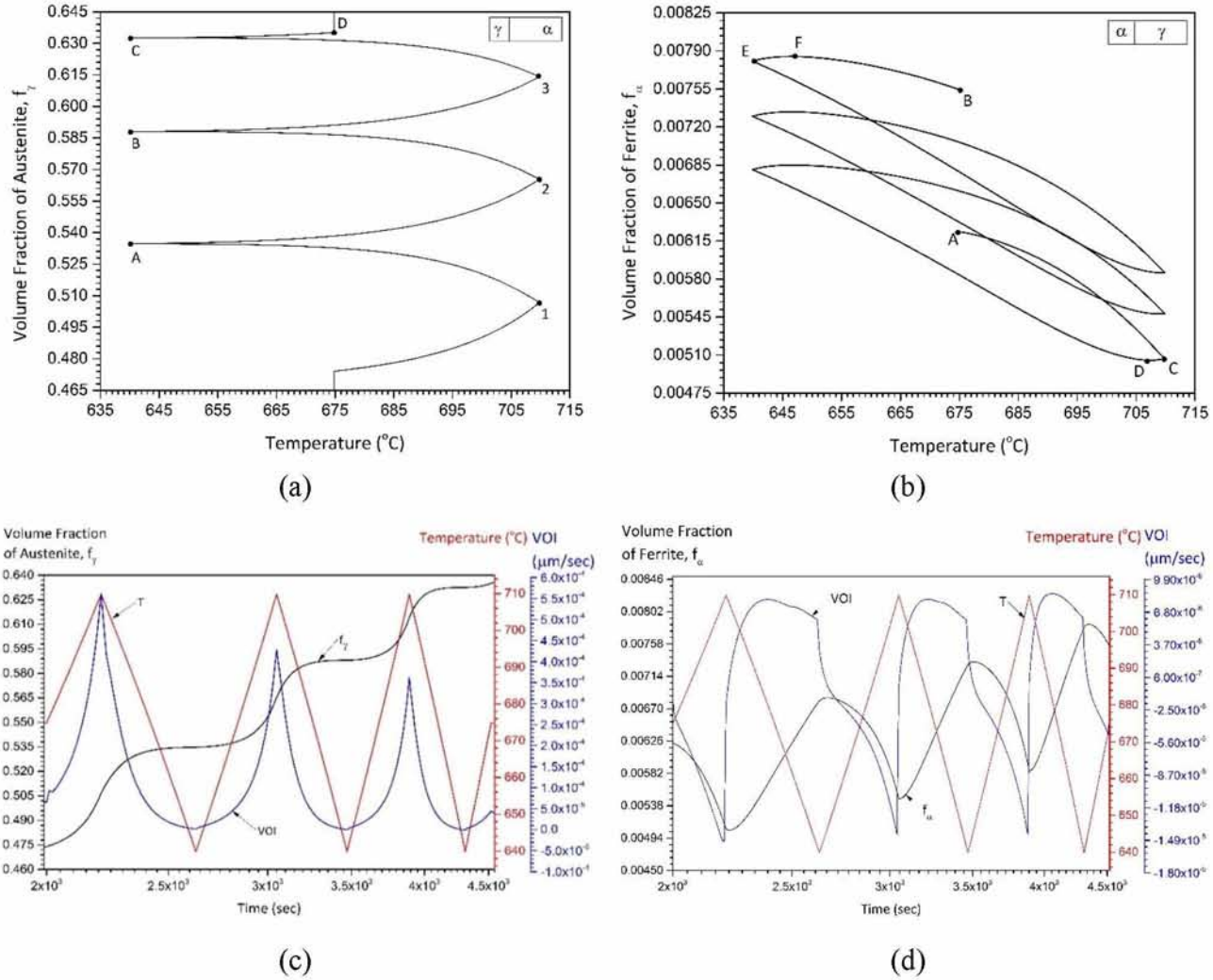

Figure 11: Cyclic transformations in Fe-0.2C-5Mn steel for $t_s=2x10^3$ sec (a) f_γ vs T for the $\alpha\rightarrow\gamma$, (b) f_α vs T for the $\gamma\rightarrow\alpha$, (c) f_γ and VOI vs time for the $\alpha\rightarrow\gamma$ and (d) f_α, VOI vs time for the $\gamma\rightarrow\alpha$ transformations.

3.1.2.2. Fe-0.2C and Fe-0.2C-0.2Mn steels

The isothermal transformations for the two steels are shown in Figure 12a and 12b. The kinetics of ferrite formation is much faster than in the Fe-0.2C-5Mn steel. The times t_s indicating the start of the cyclic transformations are indicated by dotted lines.

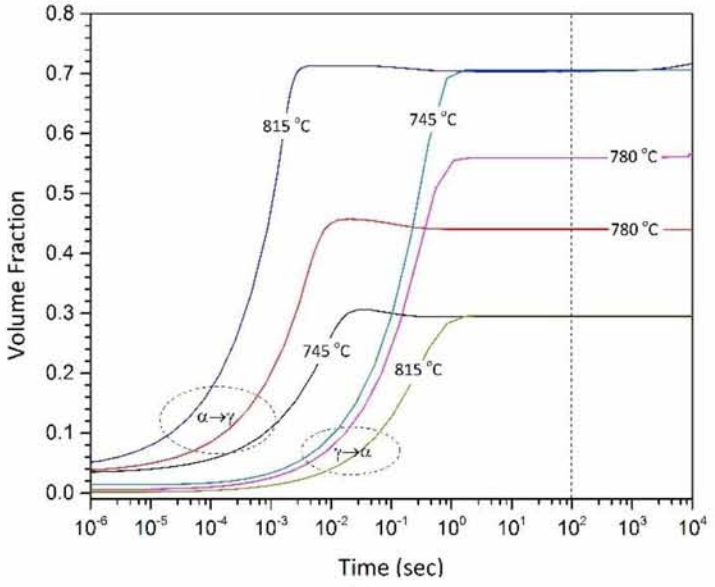

(a)

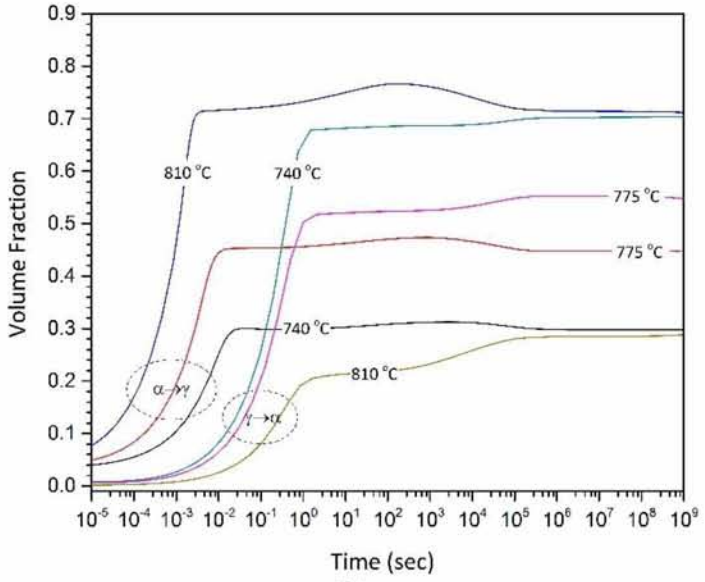

(b)

Figure 12: Isothermal transformation kinetics for (a) Fe-0.2C and (b) Fe-0.2C-0.2Mn steels.

The cyclic transformations (volume fraction vs temperature) for the two cases $\alpha \rightarrow \gamma$ and $\gamma \rightarrow \alpha$ for the Fe-0.2C and Fe-0.2C-0.2Mn steels are shown in Figure 13a and 13b for t_s=100 sec and t_s=1x10^7 sec respectively, corresponding to times where equilibrium fractions have been established in the respective isothermal curves. In the case of Fe-0.2C steel containing no manganese, the transformation is reversible and no hysteresis loops are formed. This is due to

the fast diffusion of carbon, establishing global equilibrium conditions quickly. In the case of the steel containing 0.2Mn, a hysteresis loop forms during cycling transformation. The width of the loop, in the temperature axis, is smaller than the loops in the 5Mn steel. Obviously the partitioning of manganese during the cyclic transformations is the controlling factor for loop formation and inverse transformation stages. This issue will be discussed in the next section.

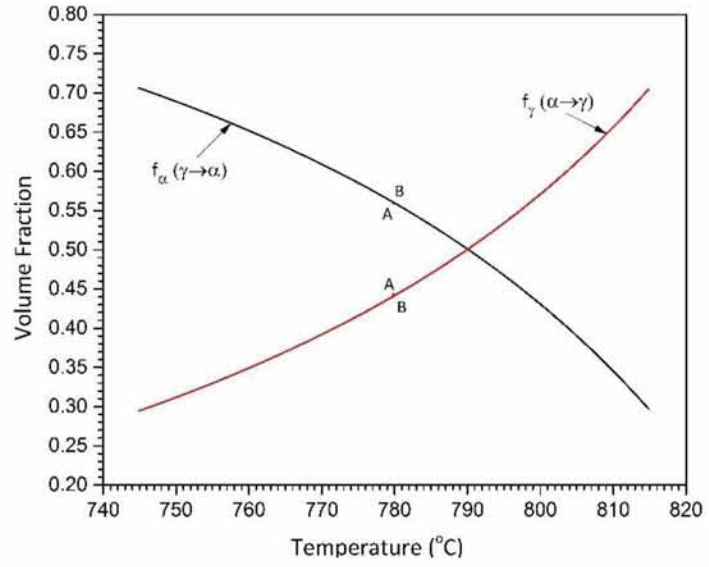

(a)

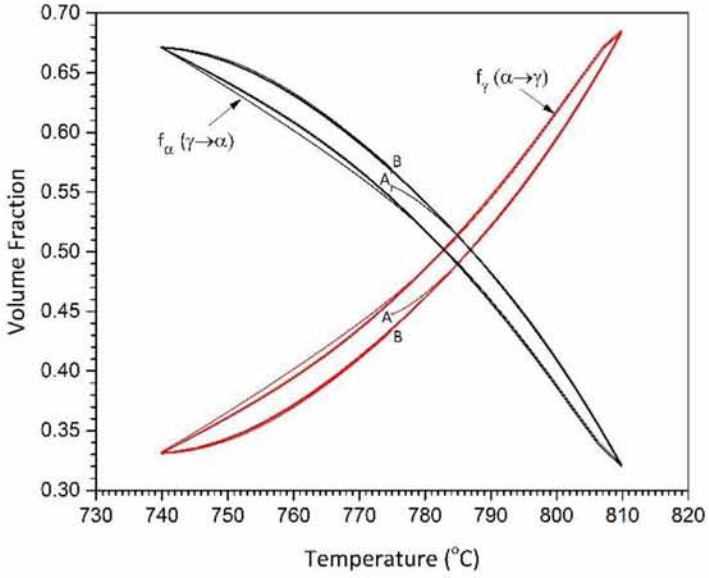

(b)

Figure 13: Cyclic transformations, volume fractions f_α and f_γ vs T for (a) Fe-0.2C and (b) Fe-0.2C-0.2Mn steels for both $\alpha \rightarrow \gamma$ and $\gamma \rightarrow \alpha$ transformations.

3.2. Solute Partitioning

The experimental validation of the simulation regarding the evolution of the austenite volume fraction, allows to apply the method in order to simulate the evolution of solute partitioning during the cyclic transformation. For the case of 4.5Mn steel during the $\alpha \rightarrow \gamma$ transformation, the solute partitioning of Mn and C is described when the starting time of the thermal treatment is before the final phase equilibrium. The evolution of the Mn profile during the first cycle is depicted in Figure 14a-d, where Figure 14a corresponds to the start of the cycle at T_{is} (686°C), Figure 14b corresponds to T_{max} (721°C), Figure 14c corresponds to T_{is} (686°C) and Figure 14d corresponds to T_{min} (651°C).

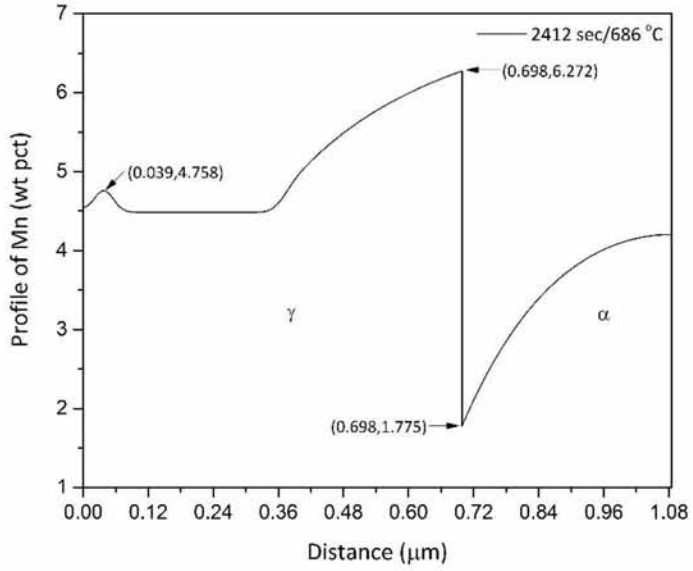

(a)

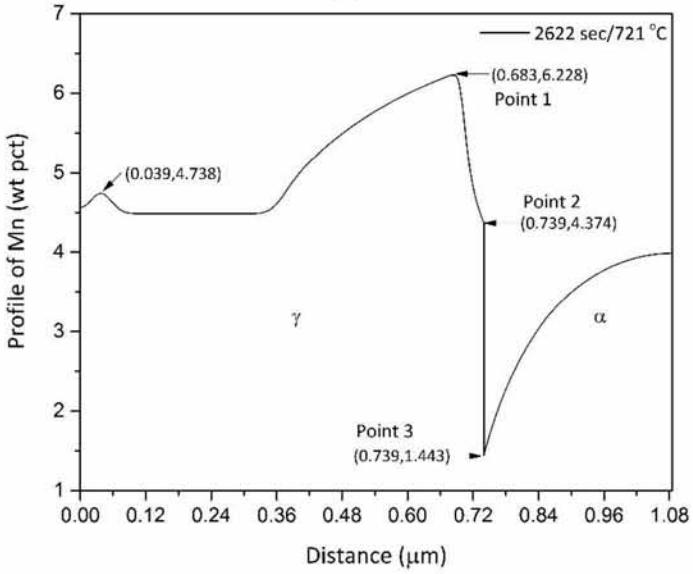

(b)

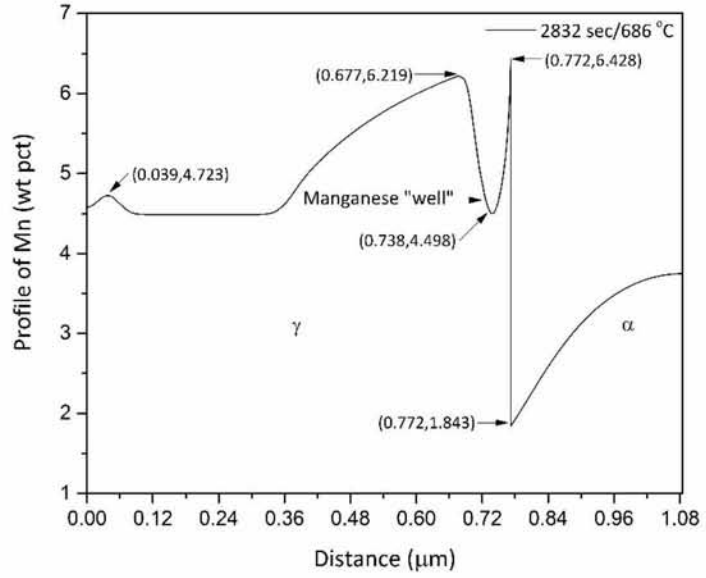

(c)

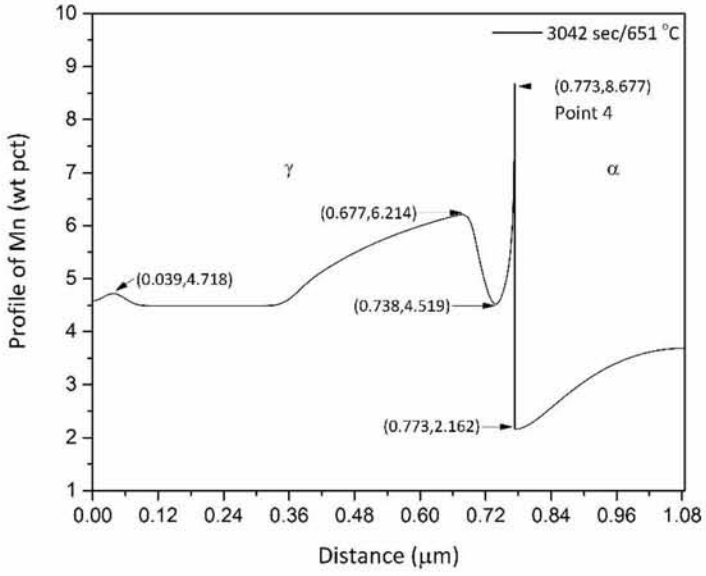

(d)

Figure 14: Evolution of the manganese profile during the first cycle of the $\alpha \rightarrow \gamma$ transformation: (a) and (b) during heating, (c) and (d) during cooling, for the times/temperatures indicated. The austenite and ferrite regions are on the left and right of the interface, respectively. The manganese 'well' is depicted in (c).

During heating, between T_{is} and T_{max}, austenite forms by forward transformation, The Mn concentration of austenite at the α/γ interface decreases leaving a peak at point 1, as shown in Figure 14b. Points 2 and 3 in Figure 14b correspond to the Mn compositions of austenite and ferrite at the interface at T_{max} according to the local equilibrium conditions. Thus the built-up of the Mn profile in austenite during heating from T_{is} to T_{max} corresponds to the line between point 1 and point 2 in Figure 14b. During cooling from T_{max} to the intermediate temperature T_{is} and then to T_{min}, shown in Figures 14c and 14d, the inverse transformation takes place and the interface continues to proceed forward. The Mn concentration in austenite at the α/γ interface

increases and the Mn profile in austenite forms a "well". The "well" corresponds to the locus of the equilibrium Mn composition in austenite at the α/γ interface, as the interfacial compositions change during thermal cycling. During heating, the Mn composition at the interface decreases while during cooling it increases, forming the "well". At T_{min}, a "stagnant" stage is observed where the shift of the interface negligible. Point 4 in Figure 14d corresponds to the Mn composition in austenite at the α/γ interface according to local equilibrium. The same behavior is repeated in the second and third cycle. It is important to note that Mn partitioning follows a similar behavior both during the forward and inverse transformations, i.e. Mn diffuses from ferrite to austenite and the transformation rate is controlled by the Mn diffusion in ferrite.

Carbon exhibits a similar behavior to Mn, although the composition fluctuations are smaller. The evolution of the carbon profiles in the first cycle, are depicted in Figure 15. A carbon "well" forms in austenite. The compositions of the well correspond to the local equilibrium compositions of carbon in austenite at the α/γ interface, which change during the thermal cycle. In contrast to Mn, the concentration of C in ferrite becomes homogeneous due to the faster diffusion of C in ferrite.

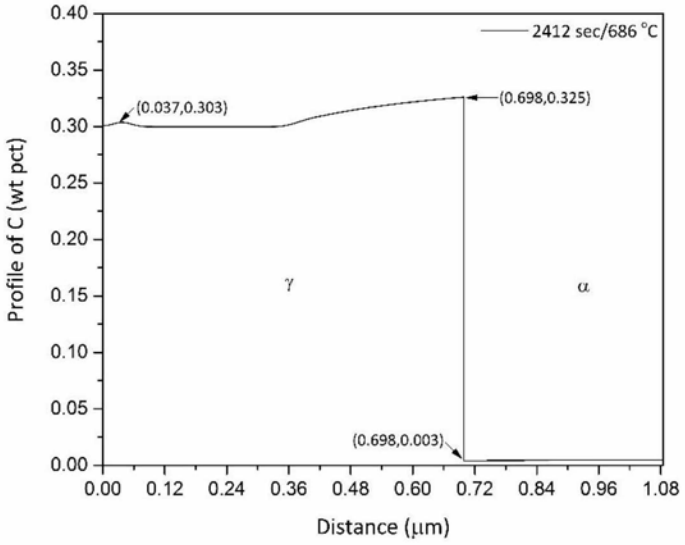

(a)

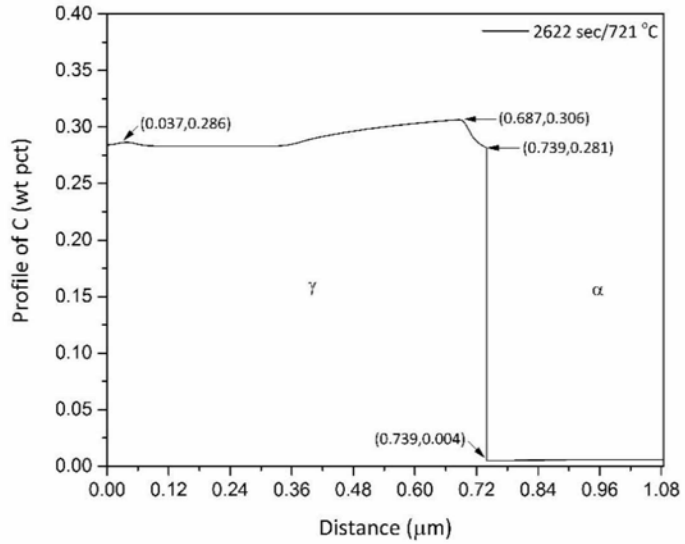

(b)

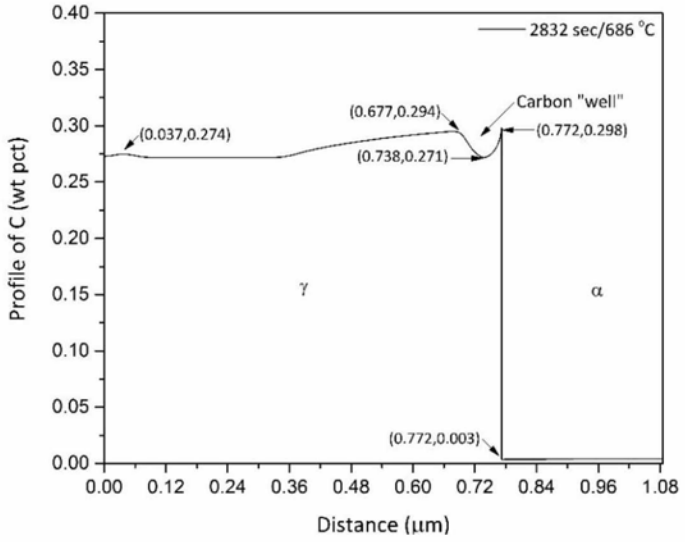

(c)

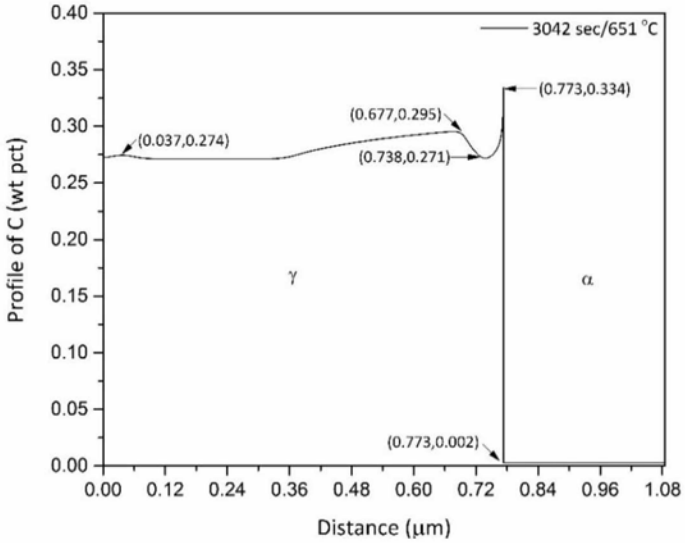

(d)

Figure 15: Evolution of the carbon profile during the first cycle of the $\alpha \rightarrow \gamma$ transformation: (a) and (b) during heating, (c) and (d) during cooling, for the times/temperatures indicated. The austenite and ferrite regions are on the left and right of the interface, respectively. The carbon 'well' is depicted in (c).

The Mn and C profiles at the end of the third cycle are depicted in Figure 16. Three wells have formed corresponding to the three cycles. The Mn "wells" are not homogenized due to the low diffusivity of Mn in austenite. This leads to the formation of a Mn layered segregation profile, exhibiting maxima and minima in composition, as a result of thermal cycling. The same holds for carbon, although some homogenization is apparent in the time period of the three cycles.

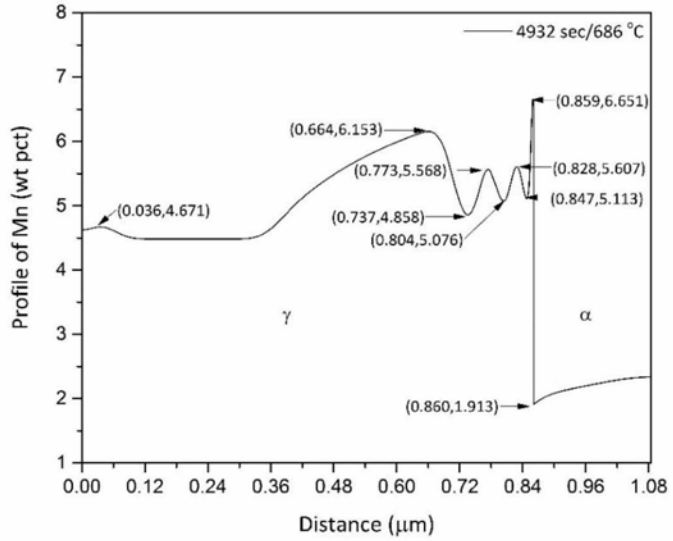

(a)

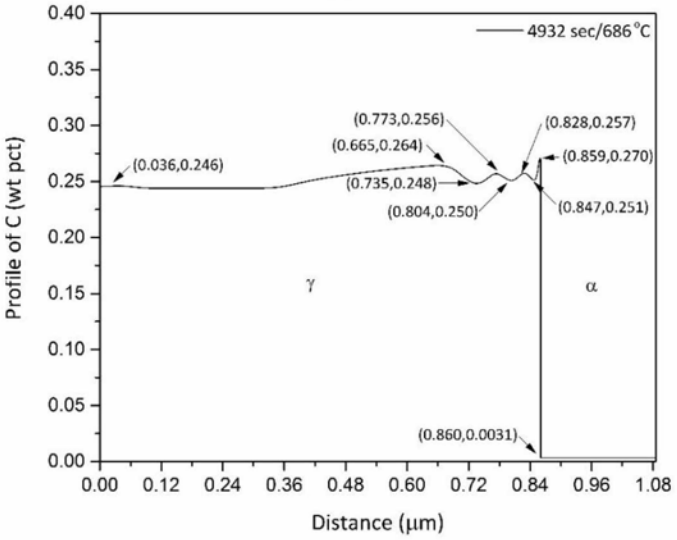

(b)

Figure 16: Profiles of (a) manganese and (b) carbon after the three cycles of the cyclic transformation. The formation of three 'wells' is indicated.

The Mn and C spikes appearing at the start of the isothermal holding, at the location 0.039μm in Figures 14 and 15 are compositional spikes, which form due to the NPLE conditions prevailing at the beginning of the isothermal transformation. The evolution of these compositional spikes has been described in detail [23, 24].

For the case of 5Mn steel during the $\gamma \rightarrow \alpha$ transformation and a starting time $t_s=2x10^3$ sec, the profiles of Mn and C magnified near the α/γ interface during the first cycle, are depicted in Figures 17 and 18 respectively. Figures 17a and 18a correspond to the start of the cycle at T_{is} (675°C), Figures 17b and 18b correspond to T_{max} (710°C) while Figures 17d and 18d correspond to T_{min} (640 °C). In Figures 17c, 18c and 17e, 18e the end of the inverse transformation is depicted at T (708.3 °C) and T (646. 6 °C) respectively. The Mn and C profiles at the end of the third cycle are depicted in Figures 17f and 18f.

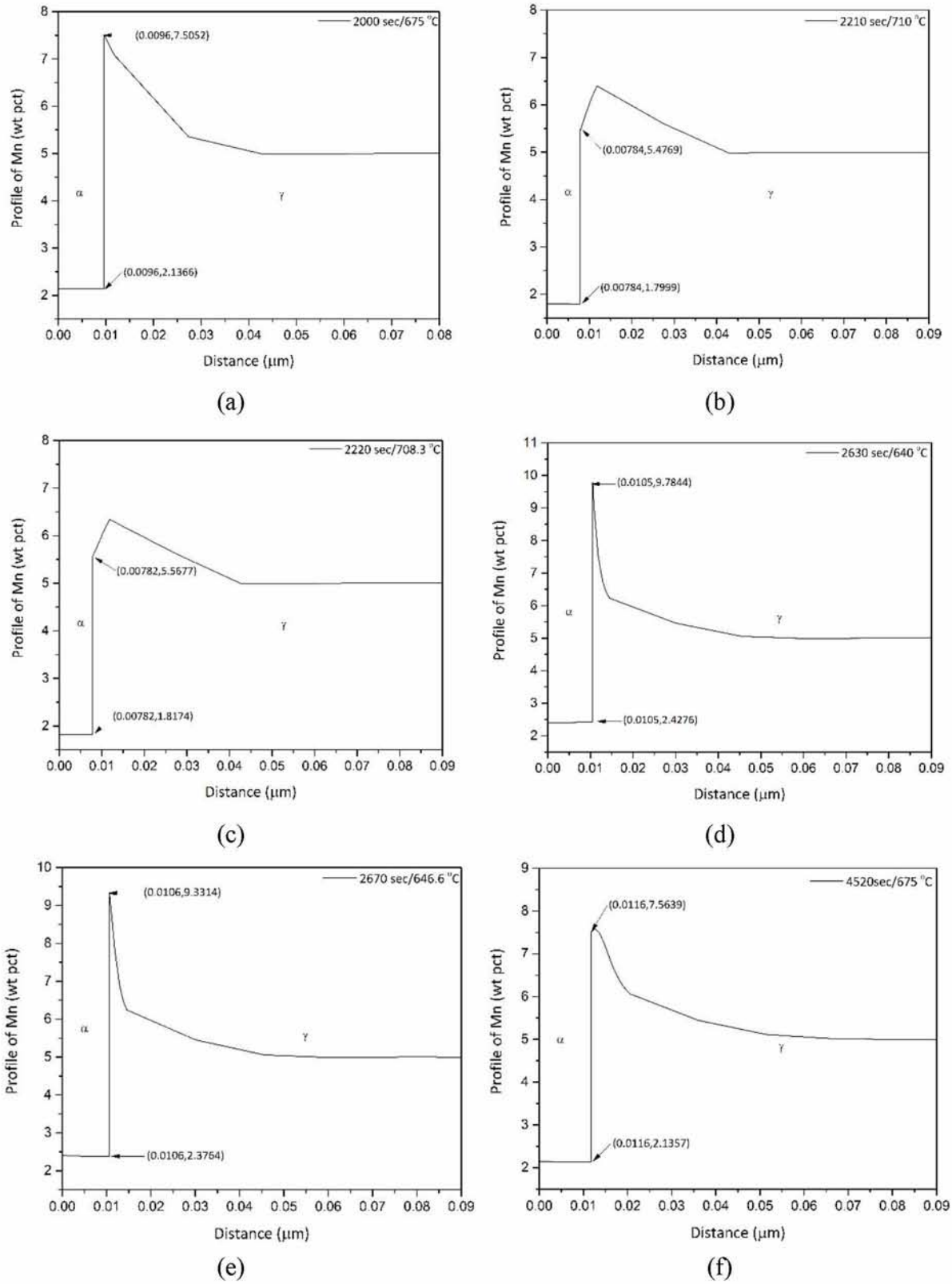

Figure 17: Evolution of the manganese profile during the first cycle of the $\gamma \rightarrow \alpha$ transformation: (a), (b) and (e) during heating, (c) and (d) during cooling, for the times/temperatures indicated. Profile of manganese after the three cycles of the cyclic transformation (f). The ferrite and austenite regions are on the left and right of the interface, respectively.

During heating, between T_{is} and T_{max}, the α/γ interface proceeds backward and austenite forms in expense of ferrite. The Mn concentration at α/γ interface in austenite decreases and obtains its lowest value at T_{max}, as shown in Figure 18a and 18b. During cooling between, T_{max} and T (708.3 °C) the inverse transformation takes place and the α/γ interface continuous to proceed slightly backward, whereas the concentration of Mn at the α/γ interface in austenite increases as depicted in Figure 18c. After the inverse stage, ferrite forms with forward transformation until T_{min}. The Mn profile at T_{min} obtains the maximum concentration at the α/γ interface in austenite as shown in Figure 18d. During heating between T_{min} and T (646.6 °C), the inverse transformation takes place and ferrite continuous to form (Figure 18e). The Mn profile at the end of the third cycle is depicted in Figure 18f. It is interesting to see that there is no formation of Mn "wells", in contrast to the $\alpha \rightarrow \gamma$ case (Figure 16). This behavior can be explained by the isothermal volume fractions of the $\alpha \rightarrow \gamma$ and $\gamma \rightarrow \alpha$ transformations shown in Figure 8, where the $\gamma \rightarrow \alpha$ transformation is much slower compared to the $\alpha \rightarrow \gamma$ transformation. Furthermore, Mn and C diffusion is faster in ferrite than in austenite. Therefore the driving force of ferrite formation is smaller and there is no formation of Mn layered segregation profile.

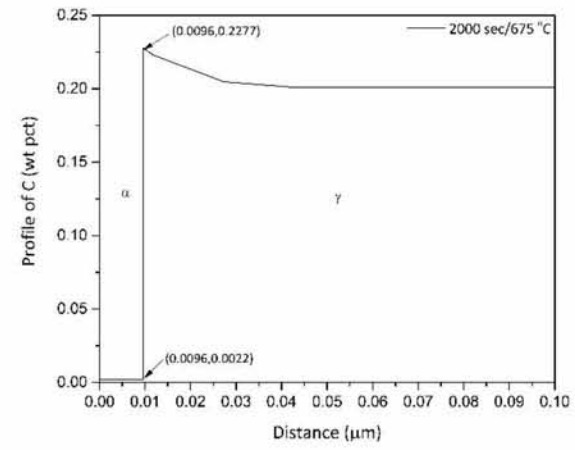

(a)

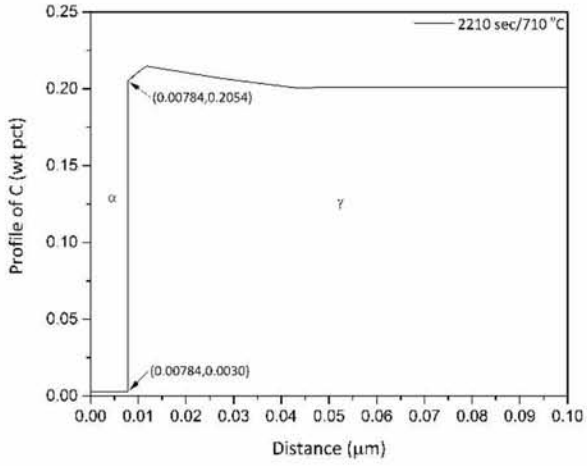

(b)

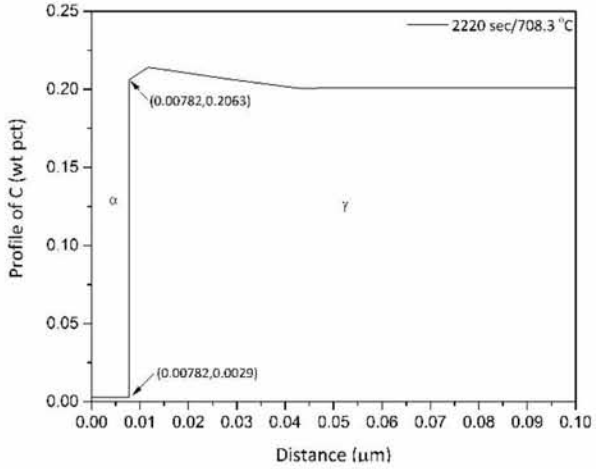

(c)

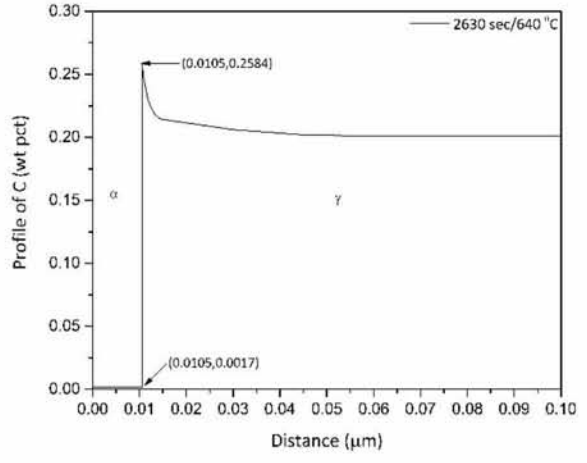

(d)

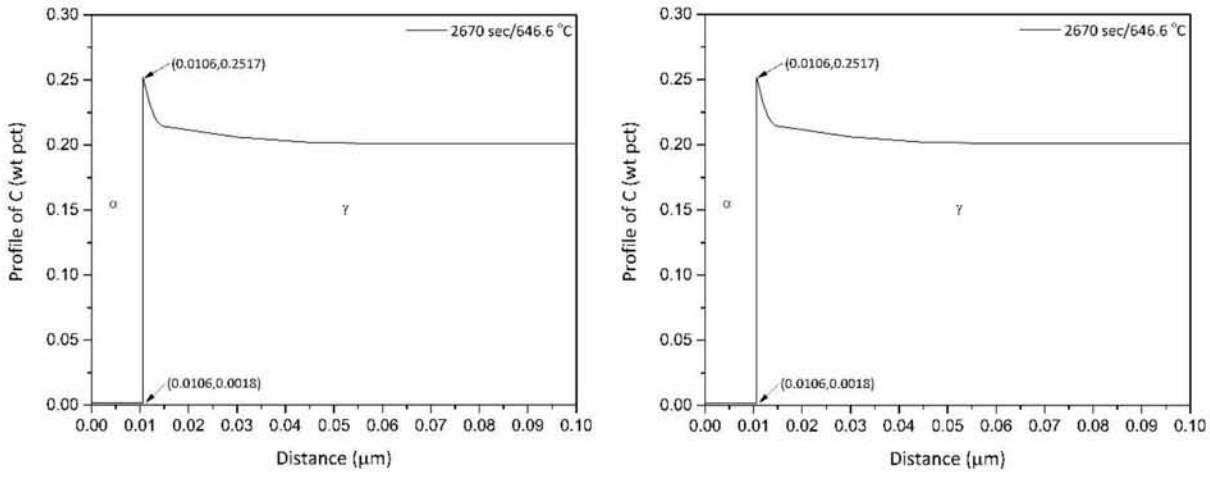

(e) (f)

Figure 18: Evolution of the carbon profile during the first cycle of the γ→α transformation: (a), (b) and (e) during heating, (c) and (d) during cooling, for the times/temperatures indicated. Profile of carbon after the three cycles of the cyclic transformation (f). The ferrite and austenite regions are on the left and right of the interface, respectively.

Carbon exhibits a similar behavior to Mn. Although the compositions fluctuations of C are smaller due to its higher diffusivity in austenite and ferrite. In addition, the concentration of C in ferrite becomes homogeneous compared to Mn concentration. The partitioning of Mn and C follows a similar behavior both during the forward and inverse transformations, i.e. Mn diffuses from ferrite to austenite and the transformation rate is controlled by the Mn diffusion in ferrite.

The solute partitioning of Mn and C for a starting time after thermodynamic equilibrium has been established in the isothermal curves, was considered for the 5Mn steel during the α→γ and γ→α transformations. For the case of α→γ transformation and a starting time $t_s=1x10^8$ sec, the profiles of Mn and C during the first cycle, are depicted in Figure 19 and 20 respectively. During the heating, between T_{is} and T_{max} the α/γ interface proceeds forward and austenite forms (Figure 19a-b and 20a-b). During cooling between T_{max} and T (700.56 °C), the inverse transformation takes place and austenite continuous to form, while the concentration of Mn and C at the α/γ interface in austenite increases (Figure 19c and 20c). With the progress of cooling until T_{min} the volume fraction of austenite decreases according to the forward transformation. The Mn and C profiles at T_{min} obtain the maximum concentration at the α/γ interface in austenite, as shown in Figure 19d and 20d respectively. During heating between T_{min} and T (659.61 °C), the inverse transformation takes place and austenite continuous to dissolve (Figure 19e and 20e). The Mn and C at the end of the third cycle are depicted in Figures 19f and 20f respectively. The profiles of Mn and C are homogenized and there is no formation of Mn and C "wells". The transformation rate is controlled by Mn diffusion in austenite (PLE stage III).

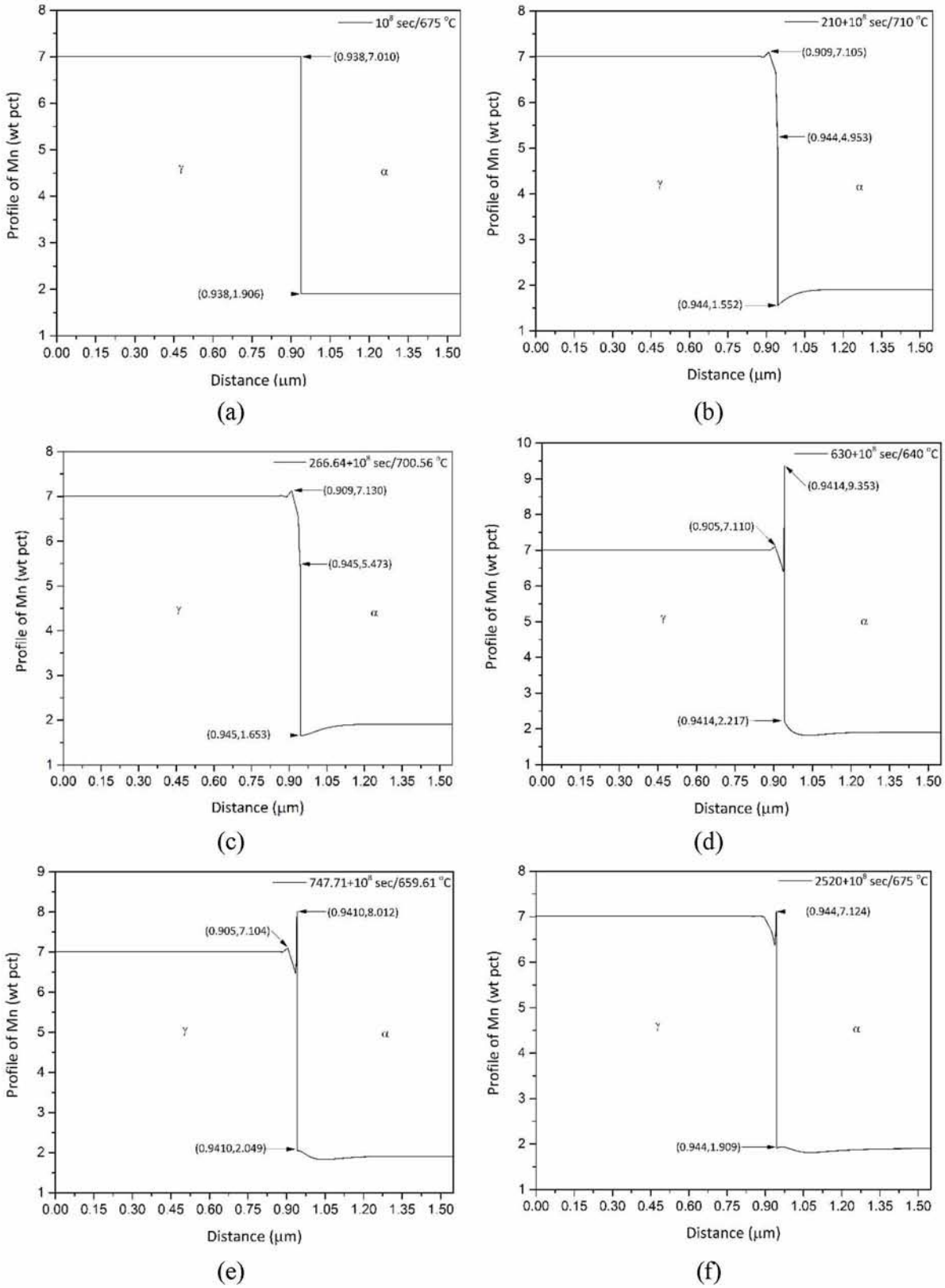

Figure 19: Evolution of the manganese profile during the first cycle of the $\alpha \rightarrow \gamma$ transformation: (a), (b) and (e) during heating, (c) and (d) during cooling, for the times/temperatures indicated. Profile of manganese after the three cycles of the cyclic transformation (f). The austenite and ferrite regions are on the left and right of the interface, respectively.

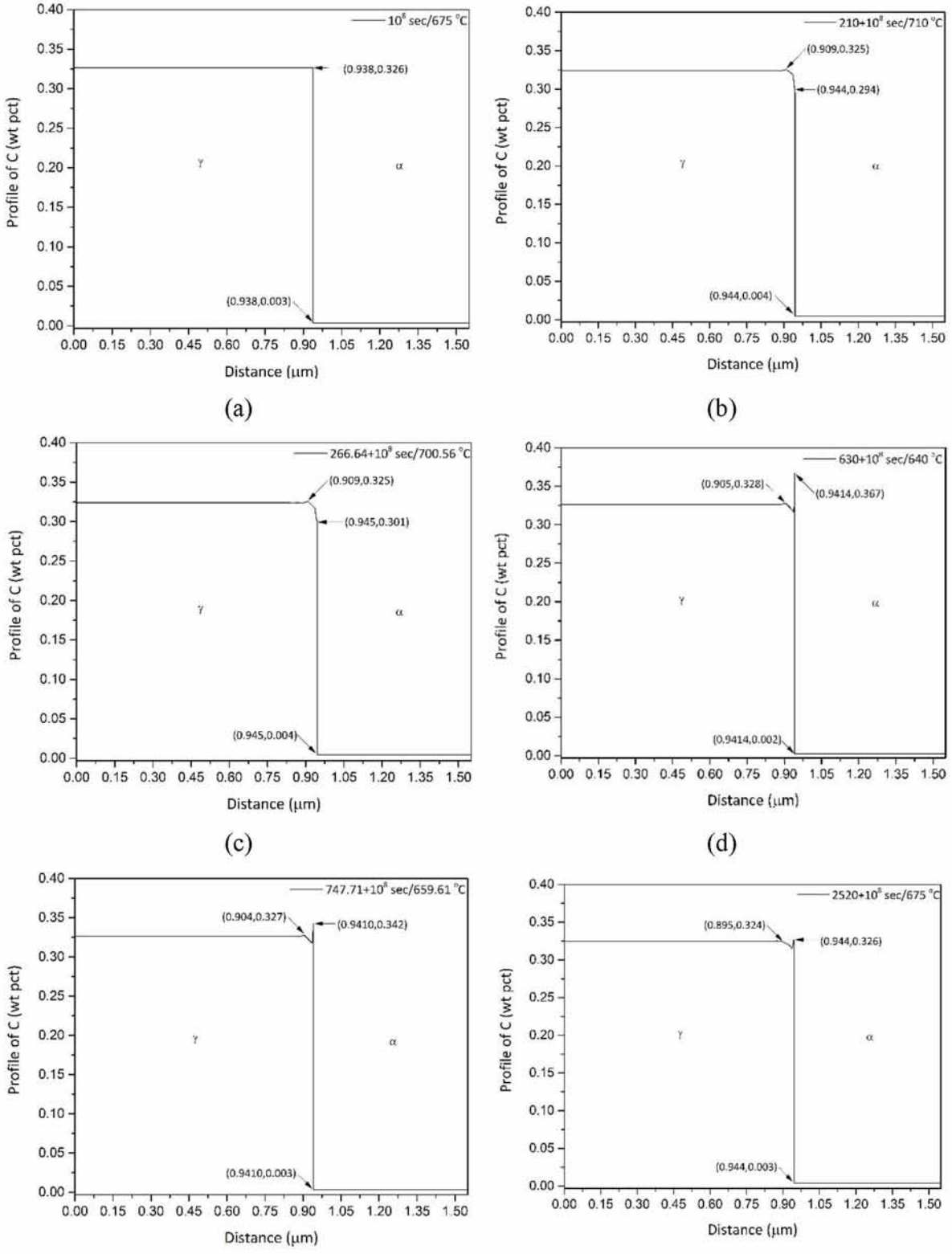

Figure 20: Evolution of the carbon profile during the first cycle of the $\alpha \rightarrow \gamma$ transformation: (a), (b) and (e) during heating, (c) and (d) during cooling, for the times/temperatures indicated. Profile of carbon after the three cycles of the cyclic transformation (f). The austenite and ferrite regions are on the left and right of the interface, respectively.

For the case of $\alpha \rightarrow \gamma$ transformation and a starting time $t_s=1x10^8$ sec, the profiles of Mn and C during the first cycle, are depicted in Figure 21a-e and 22a-e respectively. Figures 21a and 22a correspond to the start of the cycle at T_{is} (675°C), Figures 21b and 22b correspond to T_{max} (710°C) while Figures 21d and 22d correspond to T_{min} (640 °C). In Figures 21c, 22c and 21e, 22e the end of the inverse transformation is depicted at T (700.72 °C) and T (659.95 °C) respectively. The profiles of Mn and C at the end of the third cycle are shown in Figure 21f and 22f accordingly. During thermal cycling, the phase fractions form by forward and inverse transformations. At the end of the third cycle the α/γ interface has shifted backward, indicating that the volume fraction of ferrite has been decreased. The profiles both of Mn and C are homogenized and there is no formation of Mn and C "wells". The transformation rate is controlled by Mn diffusion in austenite (PLE stage III).

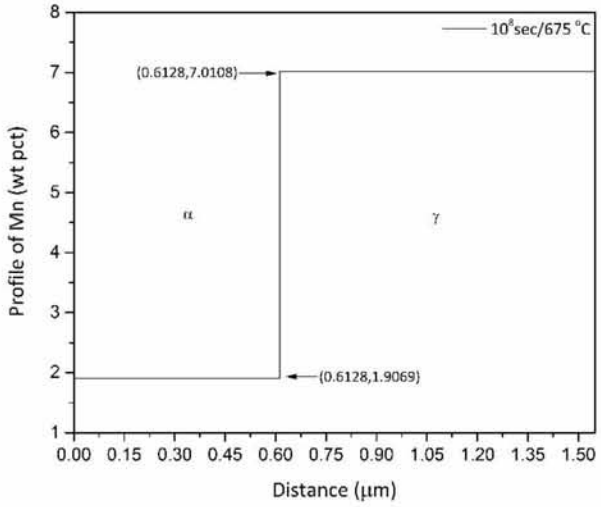

(a)

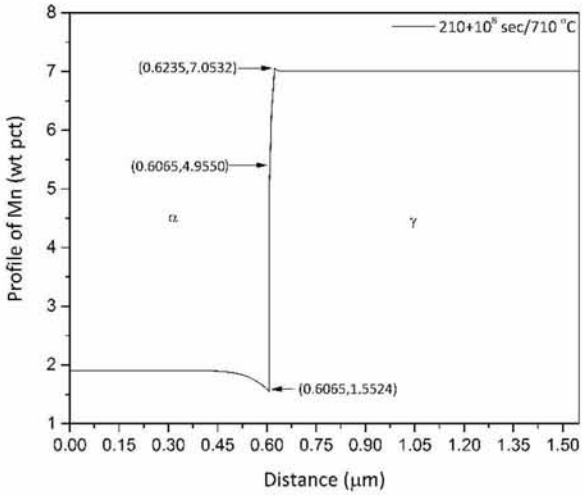

(b)

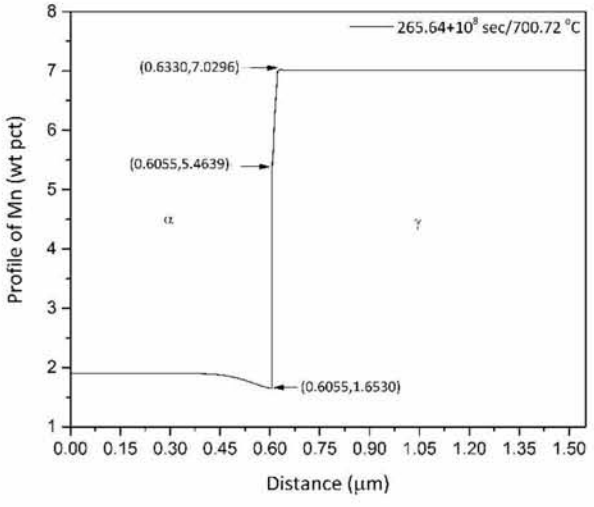

(c)

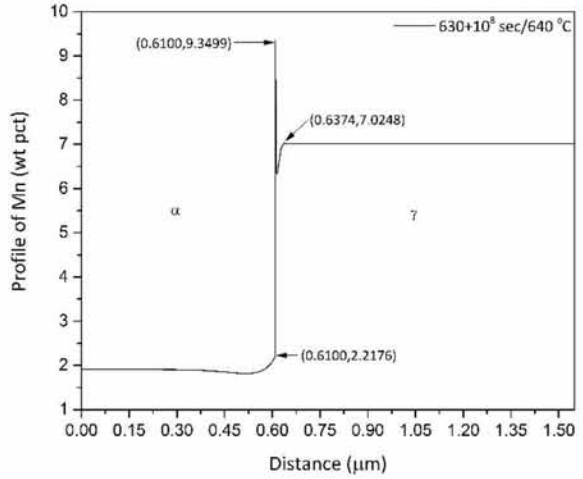

(d)

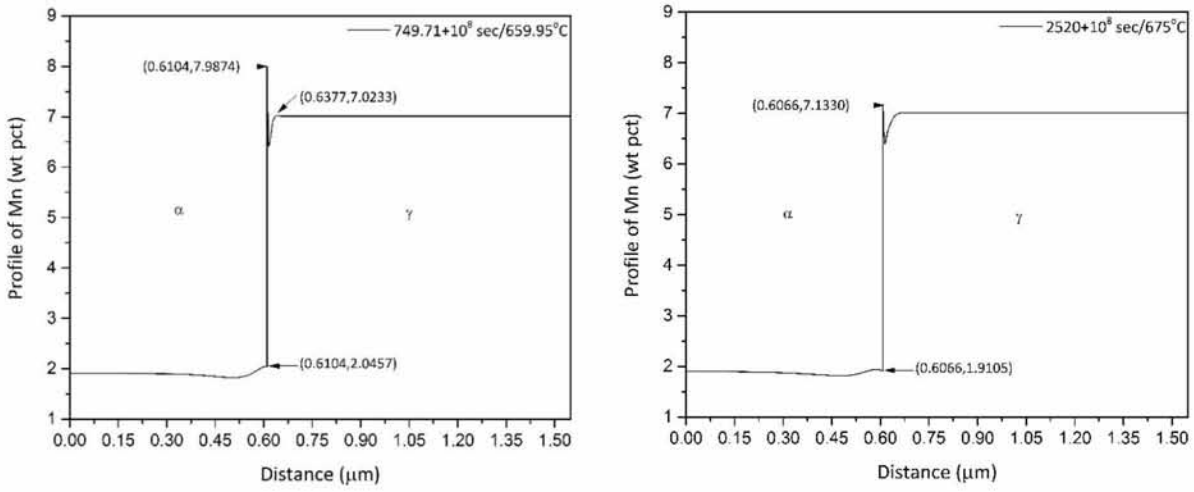

(e) (f)

Figure 21: Evolution of the manganese profile during the first cycle of the γ→α transformation: (a), (b) and (e) during heating, (c) and (d) during cooling, for the times/temperatures indicated. Profile of manganese after the three cycles of the cyclic transformation (f). The ferrite and austenite regions are on the left and right of the interface, respectively.

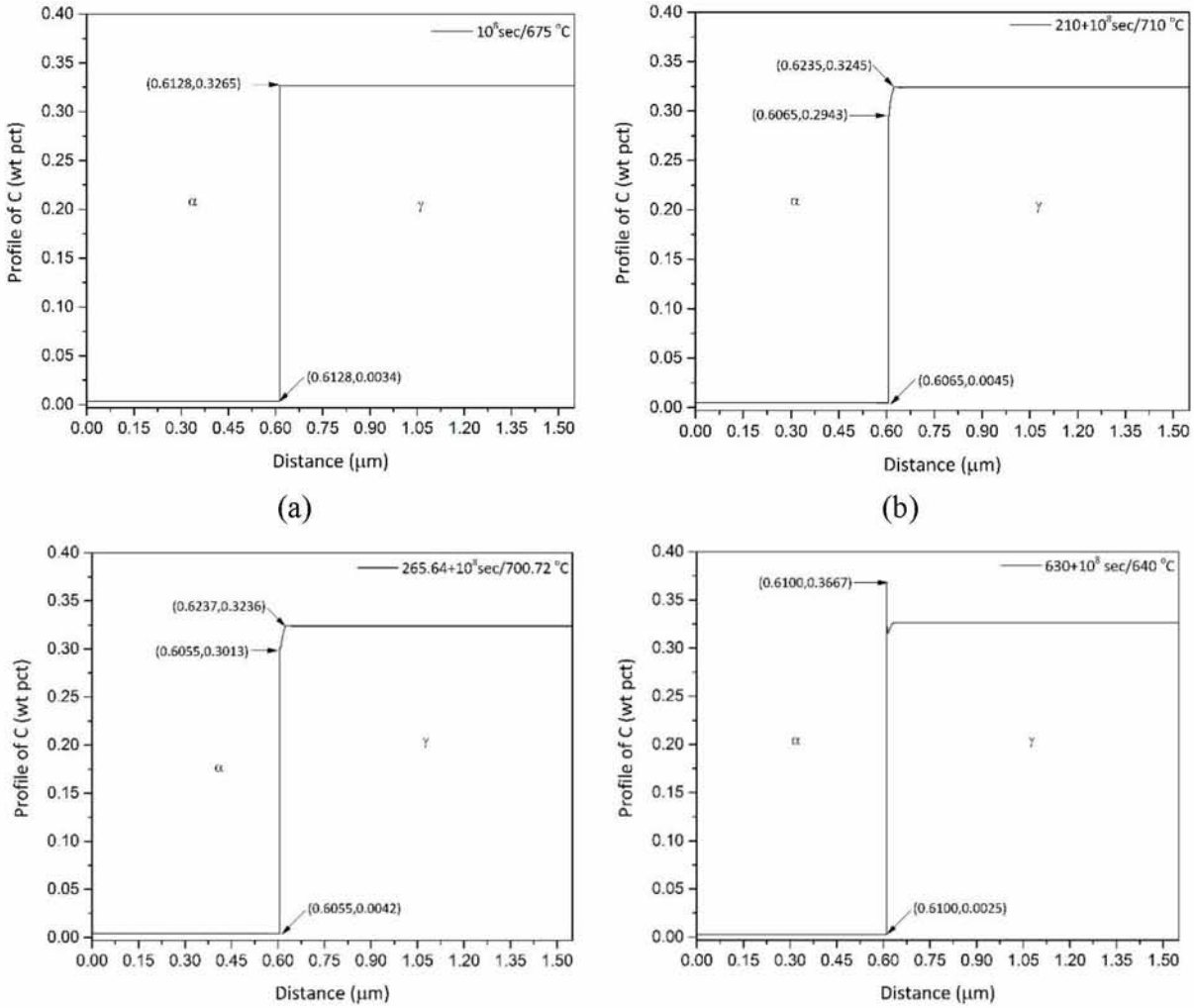

(a) (b)

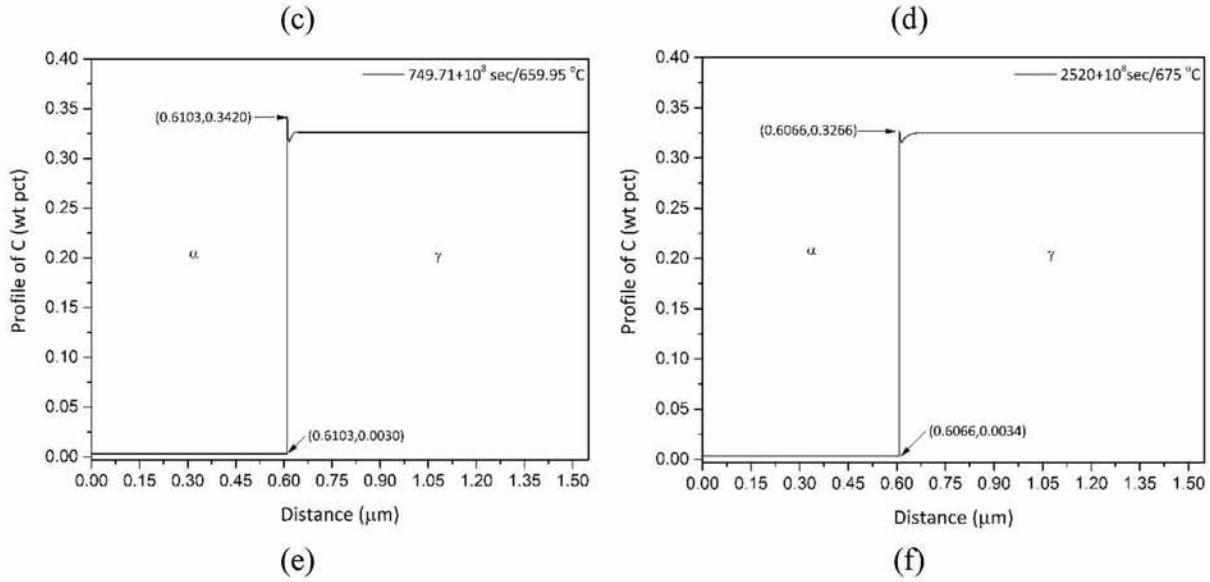

Figure 22: Evolution of the carbon profile during the first cycle of the γ→α transformation: (a), (b) and (e) during heating, (c) and (d) during cooling, for the times/temperatures indicated. Profile of carbon after the three cycles of the cyclic transformation (f). The ferrite and austenite regions are on the left and right of the interface, respectively.

4. CONCLUSIONS

Cyclic phase transformations were simulated in Fe-0.2C-4.5Mn and Fe-0.2C-5Mn steels as well as in Fe-0.2C and Fe-0.2C-0.2Mn (mass%) steels for comparison, during thermal cycling in the intercritical range. Solute partitioning of Mn an C have been studied for the Fe-0.2C-4.5Mn (mass%) steel for a case where the starting time of the cyclic treatment is well before the equilibrium fractions have been established in the respective isothermal intercritical treatment. From the results of the simulations and experiments, the following conclusions can be drawn.

1. The evolution of austenite during thermal cycling in the intercritical range comprises of forward, inverse and stagnant stages. The simulation results have been experimentally validated by dilatometry for the case of Fe-0.2C-4.5Mn steel.
2. The cyclic behavior for a specific steel composition depends on the starting time of the cyclic treatment relative to the isothermal transformation curve.
3. When the cyclic treatment is performed after the equilibrium phase fractions during isothermal treatment have been established, hysteresis loops form in the Fe-0.2C-5Mn and Fe-0.2C-0.2Mn steels. The cyclic behavior is fully reversible for the Fe-0.2C steel.
4. The inverse transformation stage has been investigated for the Fe-0.2C-5Mn steel. For a starting time after the equilibrium phase fractions have been established, the duration of the inverse transformation stage is larger at the minimum temperature of the cycle. The phase fraction formed during the inverse transformation is larger at the maximum temperature of the cycle. For a starting time before thermodynamic equilibrium, the duration of the inverse transformation stage is larger at the minimum temperature of the

cycle, whereas the phase fraction formed is approximately equal both at the maximum and minimum temperatures of the cycle.

5. In Fe-0.2C-5Mn and Fe-0.2C-4.5Mn steels for the $\alpha \rightarrow \gamma$ case, when thermal cycling takes place at a time before the final phase equilibrium in the isothermal curve, austenite formation proceeds with the forward transformation during the heating part and with the inverse transformation during the whole cooling part of the cycle. Both transformations take place at comparable rates. The fraction of austenite formed decreases in each successive cycle due to a corresponding decrease of the transformation rate.
6. A stagnant stage, where the transformation is very sluggish was observed during the cyclic transformations for the steels investigated.
7. For a starting time before the final phase equilibrium, the kinetics of austenite and ferrite evolution during the cyclic transformation is controlled by the Mn diffusion in ferrite, both for the forward and the inverse transformations. For a starting time after the final phase equilibrium, the transformation rate is controlled by Mn diffusion in austenite.
8. For the $\alpha \rightarrow \gamma$ case and a starting time before final phase equilibrium, partitioning of Mn and C take place from ferrite to austenite during the cyclic transformation. Due to the low diffusivity in austenite, wells form in the composition profiles in austenite of both Mn and C. These wells are the locus of the interfacial compositions of austenite corresponding to the variation of the local equilibrium conditions during the thermal cycle.
9. The wells in the composition profiles correspond to the formation of a layered segregation in austenite, exhibiting maxima and minima, as the result of the cyclic thermal treatment in the intercritical range.
10. For a starting time after thermodynamic equilibrium there is no formation of Mn and C wells. The same holds for the $\gamma \rightarrow \alpha$ case for a starting time before the final phase equilibrium, due to the sluggish transformation rate of ferrite.

5. SUGGESTIONS FOR FUTURE RESEARCH

1. The influence of other elements (Al, Si, Ni) during the cyclic transformation and solute partitioning in the intercritical range.
2. The quantification of Mn effect during the inverse and the stagnant stages, as well as the proportion of Mn and C needed for the appearance of inverse behavior.
3. Further experimental validation. For example an EDS analysis or an atom probe tomography for the measurement of Mn and C profiles during the solute partitioning in the intercritical range.
4. Development of steel microstructures from layered segregated profiles.

BIBLIOGRAPHY

1. Matlock DK and Speer JG (2009) *Third Generation of AHSS: Microstructure Design Concepts, in Microstructure and Texture in Steels*, A Haldar, S Suwas, and D Bhattacharjee, Editors, Springer London.
2. Matlock DK, Speer J, De Moor E and Gibbs PJ (2012) Recent developments in advanced high strength sheet steels for an automotive application: an overview, *JESTECH*, 15:1-12.
3. Suh DW, Ryu JH, Joo MS, Yang HS, Lee K, and Bhadeshia HKDH (2012) Medium-Alloy Manganese-Rich Transformation-Induced Plasticity Steels. *Metall. Mater. Trans.* (A) 44: 286-293.
4. Lee S-J, Lee S and De Cooman BC (2011) Austenite stability of ultrafine-grained transformation-induced plasticity steel with Mn partitioning, *Scr. Mater.*, 65:225–228
5. Zackay VF, Parker ER, Fahr D and Bush R (1967) The enhancement of ductility in high-strength steels. *Trans. Am. Soc. Met.*, 60, 252-259.
6. Matsumura O, Sakuma Y and Takechi Y (1987) Enhancement of elongation by retained austenitein intercritical annealed 0.4C-1.5Si-0.8Mn steel. *Trans. ISIJ*, 27:570-579.
7. Speer JG, Assunção FCR, Matlock DK, and Edmonds DV (2005) The "quenching and partitioning" process: background and recent progress. *Materials Research,* 8:417-423.
8. Edmonds DV, He K, Rizzo FC, De Cooman BC, Matlock DK and Speer JG (2006) Quenching and partitioning martensite-A novel steel heat treatment. *Mater. Sci. Eng.*, (A) 438-440, 25-34.
9. Kamoutsi H, Gioti E, Haidemenopoulos GN, Cai Z and Ding H (2015) Kinetics of solute partitioning during intercritical annealing of a medium-Mn steel. *Metall. Mater. Trans. A,* 46:4841-4846.
10. Miller RL (1972). Ultrafine-grained microstructures and mechanical properties of alloy steels. *Metall. Trans.,* 3 (4), 905-912.
11. Suh DW, Park SJ, Lee TH, Oh CS, Kim SJ (2010) Influence of Al on microstructure and mechanical behavior of low carbon manganese transformation-induced plasticity steels. *Metall. Mater. Trans.* (A) 41:397-408.
12. Merwin MJ (2007), *SAE Technical Paper*, SAE, Warrendale, PA.
13. Huang H, Matsumura O and Furukawa T (1994) Retained austenite in low carbon, manganese steel after intercritical heat treatment. *Mater. Sci. Technol.*, 10:621-626.
14. Cai ZH, Ding H, Xue X and Xin QB (2013) Microstructural evolution and mechanical properties of hot-rolled 11% manganese TRIP steel. *Mater. Sci. Eng.,* (A), 560:388-395.
15. Cai ZH, Ding H, Misra RDK, Kong H and Wu HY (2014) Unique impact of ferrite in influencing austenite stability and deformation behavior in a hot-rolled Fe-Mn-Al-C steel. *Mater. Sci. Eng.*, (A), 595:86-91.
16. Chen H, Van der Zwaag S (2010) Application of the cyclic phase transformation concept for investigating growth kinetics of solid-state partitioning phase transformations. *Comp. Mater. Sci.*, 49:801-813.

17. Chen H, Appolaire B, Van der Zwaag S (2011) Application of cyclic partial phase transformations for identifying kinetic transitions during solid-state phase transformations: Experiments and modeling. *Acta Mater.,* 59:6751-6760.
18. Anderson JO, Helander T, Höglund L, Shi P and Sundman B (2002*) Thermo-Calc & DICTRA, computational tools for materials science.* Calphad, 26:273-312.
19. Borgenstam A, Hoglund L, Agren J, Engstrom A (2000) *Dictra a tool for simulation of Diffusional Transformations in Alloys*. J. Phase Equil., 21:269-280.
20. Cai Z, Ding H, Misra RDK, Ying ZY (2015) Austenite stability and deformation behavior in a cold rolled transformation-induced plasticity steel with medium manganese content. *Acta Mater.*, 84:229-236.
21. Wei R, Enomoto M, Hadian R, Zurob HS and Purdy GR (2013) Growth of austenite from as-quenched martensite during intercritical annealing in an Fe-0.1C-3Mn-1.5Si alloy. *Acta Mater.,* 61:697-707.
22. Nakada N, Mizutani K, Tsuchiyama T and Takaki S (2014) Difference in transformation behavior between ferrite and austenite formations in medium manganese steel. *Acta Mater.,* 65: 251-258.
23. Hillert M (1984). Thermodynamics of the massive transformation. *Metall. Trans. A,* 15A, 411.
24. Chen H, Zhu K, Zhao L, Van der Zwaag S (2013) Analysis of transformation stasis during the isothermal bainitic ferrite formation in Fe-C-Mn and Fe-C-Mn-Si alloys. *Acta Mater.*, 61:5458-5468.